N73-16607
NASA CR-2189

NASA CONTRACTOR REPORT

NASA CR-2189

ATMOSPHERIC ENERGETICS AS RELATED TO CYCLOGENESIS OVER THE EASTERN UNITED STATES

by Philip Walter West

Prepared by
TEXAS A & M UNIVERSITY
College Station, Texas
for George C. Marshall Space Flight Center

NATIONAL AERONAUTICS AND SPACE ADMINISTRATION • WASHINGTON, D. C. • JANUARY 1973

TECHNICAL REPORT STANDARD TITLE PAGE

1. REPORT NO.	2. GOVERNMENT ACCESSION NO.	3. RECIPIENT'S CATALOG NO.
NASA CR-2109		

4. TITLE AND SUBTITLE	5. REPORT DATE
ATMOSPHERIC ENERGETICS AS RELATED TO CYCLOGENESIS OVER THE EASTERN UNITED STATES	January 1973
	6. PERFORMING ORGANIZATION CODE

7. AUTHOR(S)	8. PERFORMING ORGANIZATION REPORT #
Philip Walter West	M108

9. PERFORMING ORGANIZATION NAME AND ADDRESS	10. WORK UNIT NO.
Texas A&M University Department of Meteorology College Station, Texas	11. CONTRACT OR GRANT NO. NAS 8-26751
	13. TYPE OF REPORT & PERIOD COVERED Contractor
12. SPONSORING AGENCY NAME AND ADDRESS National Aeronautics and Space Administration Washington, D. C. 20546	14. SPONSORING AGENCY CODE

15. SUPPLEMENTARY NOTES
Submitted to the Graduate College of Texas A&M University in partial fulfillment of the requirements for the degree of Doctor of Philosophy.

16. ABSTRACT

A method is presented to investigate the atmospheric energy budget as related to cyclogenesis. Energy budget equations are developed that are shown to be advantageous because the individual terms represent basic physical processes which produce changes in atmospheric energy, and the equations provide a means to study the interaction of the cyclone with the larger scales of motion. The work presented in this paper represents an extension of previous studies because all of the terms of the energy budget equations were evaluated throughout the development period of the cyclone. Computations are carried out over a limited atmospheric volume which encompasses the cyclone, and boundary fluxes of energy that were ignored in most previous studies are evaluated.

Two examples of cyclogenesis over the eastern United States were chosen for study. One of the cases (1-4 November, 1966) represented an example of vigorous development, while the development in the other case (5-8 December, 1969) was more modest. Objectively analyzed data were used in the evaluation of the energy budget terms in order to minimize computational errors, and an objective analysis scheme is described that insures that all of the resolution contained in the rawinsonde observations is incorporated in the analyses. While computational errors may be serious due to errors in the measured data, particularly in the higher levels of the atmosphere, it is felt that the results of this study present a representative picture of energy processes during cyclogenesis.

Results of this investigation indicate that (1) diabatic processes can be a significant factor in the development of a cyclone, (2) the downward transport of kinetic energy from the jetstream level can be an important source of energy for a developing cyclone, (3) there is considerable interaction between a cyclone and its environment, (4) the $\omega\alpha$-technique of computing conversion rates that was used in most of the previous studies may produce erroneous results because of the ommision of boundary terms, and (5) it is difficult, if not impossible, to draw generalized conclusions from the study of one or two cyclones because of the marked variability that can exist between energy processes in different cyclones.

17. KEY WORDS	18. DISTRIBUTION STATEMENT

19. SECURITY CLASSIF. (of this report)	20. SECURITY CLASSIF. (of this page)	21. NO. OF PAGES	22. PRICE
Unclassified	Unclassified	126	$3.00

MSFC - Form 3292 (1

FOREWORD

This report is one of several to be published from research conducted under, or supported in part by, NASA Contract No. NAS8-26751, entitled "Atmospheric Energetics as Related to Cyclogenesis Over the Eastern United States." A number of approaches have been and continue to be followed in the conduct of the research. The results presented in this report are those from one approach, and represent only a portion of the total research effort. Other reports will be published as the research progresses.

ACKNOWLEDGMENTS

The financial support for the author's graduate program was provided by the United States Air Force under sponsorship of the Air Force Institute of Technology.

I wish to express my gratitude to Dr. James R. Scoggins who provided continuous guidance and encouragement, not only in the preparation of this dissertation, but throughout the duration of my graduate studies. I also wish to thank Dr. Vance E. Moyer, Dr. Robert A. Clark, Dr. Dusan Djuric, Dr. Don W. De Michele, and Dr. E. C. Klipple for their assistance in the final preparation of this dissertation.

Acknowledgment is extended for computer support provided by NASA under Contract No. NAS8-26751. This contract is under the auspices of the Aerospace Environment Division, Aero-Astrodynamics Laboratory, Marshall Space Flight Center, Huntsville, Alabama.

TABLE OF CONTENTS

TABLE OF CONTENTS (CONTINUED)

TABLE OF CONTENTS (CONTINUED)

LIST OF FIGURES

LIST OF FIGURES (CONTINUED)

LIST OF TABLES

LIST OF SYMBOLS

SCALARS

A	horizontal cross-sectional area of an atmospheric volume, i.e., $dA = dxdy$
$\overline{A_0}$	value of an arbitrary field at point 0 after smoothing
A_i, i=0,8	value of arbitrary field at point i
A''	dummy variable of integration that corresponds to A
c_p	specific heat at constant pressure
c_v	specific heat at constant volume
C	drag coefficient
$C(\pi, K_h)$	conversion of total potential energy into kinetic energy
$C(\pi, \pi')$	conversion of total potential energy within a volume to total potential energy in the surrounding volume
c_{ij}	total correction for grid point (i,j)
$D(K_h)$	dissipation of kinetic energy
dH/dt	diabatic heating per unit mass
E^k	error between the observation and first guess analysis at the observation location for the k^{th} observation
f	Coriolis parameter

g	acceleration due to gravity
$H(\pi)$	horizontal component of the boundary flux of total potential energy
$H(K_h)$	horizontal component of the boundary flux of kinetic energy
I	internal energy
i,j	subscripts to denote grid points
k	superscript to denote observation number
k'	von Karman constant
K	kinetic energy
p	pressure
p_1, p_2	pressures at the bottom and top of an arbitrary layer in the atmosphere
P	gravitational potential energy
r	distance between grid point and observation location
R	gas constant for dry air
SR	scan radius
T	virtual temperature (absolute)
u	wind component in x direction
U_g	geostrophic wind speed
v	wind component in y direction

LIST OF SYMBOLS (CONTINUED)

V^*	volume which encompasses the entire atmosphere
V''	dummy variable of integration for volume integrals
V	arbitrary limited volume in the atmosphere
V'	difference between V^* and V, i.e., $V' = V^* - V$
$VF(\pi)$	vertical component of the boundary flux of total potential energy
$VF(K_h)$	vertical component of the boundary flux of kinetic energy
w	vertical velocity, dz/dt
w_R	vertical velocity in a hydrostatic atmosphere
w_{ij}^k	weight for grid point (i,j) for the k^{th} observation
(x,y,z)	Cartesian coordinates
Z_0	roughness parameter
α	specific volume
γ	angular departure from the geostrophic wind and shear stress vectors
μ_h	coefficient of lateral mixing
ν	smoothing coefficient
π	total potential energy, P + I
ρ	density
ϕ	arbitrary scalar quantity
ω	vertical velocity, dp/dt

LIST OF SYMBOLS (CONTINUED)

VECTORS

$\mathbf{A}$	arbitrary vector quantity
$\mathbf{V}$	three-dimensional wind vector
$\mathbf{V}_2$	two-dimensional wind vector (vertical component excluded)
∇	three-dimensional del operator
∇_2	two-dimensional del operator (vertical component excluded)
∇_p	two-dimensional del operator on a constant pressure surface
$\mathbf{F}$	three-dimensional frictional force
$\mathbf{F}_2$	two-dimensional frictional force (vertical component excluded)

1. INTRODUCTION

a. Statement of the problem

While meteorologists have long realized that the migratory extratropical disturbances are areas where energy conversions are maximized, the exact mechanisms that effect the conversions between kinetic, internal, and gravitational potential energy have remained somewhat obscure. In particular, the determination of how and where these conversions take place in a developing cyclone is still a fundamental problem in meteorology.

Comprehensive studies of the energy processes in individual synoptic systems have been limited primarily because of the difficulties in evaluating the boundary integrals that can represent a significant portion of the energy budget. The existence of non-zero boundary integrals also complicates the interpretation of the energy conversion processes. These factors have resulted in a majority of the effort being directed toward specifying the global energy budget, a simpler problem because the boundary integrals become zero when the entire atmosphere is under consideration.

Quantitative studies of the energy transformations in individual cyclones are necessary in order to better understand their evolution. For example, it is desirable to learn more about the

---

The citations on the following pages follow the style of the Journal of Applied Meteorology.

energy transformations necessary to maintain the kinetic energy of the cyclone against the ever present frictional dissipation. Admittedly, energy considerations represent only one aspect of the problem, and a complete understanding of the initiation, growth, and subsequent decay of extratropical cyclones would involve the simultaneous solution of the mass, momentum, and energy relationships. However, this is an unsolvable problem with the existing knowledge and observational network.

The hypothesis underlying the research presented in this paper is that energy processes can be related to cyclogenesis through a detailed study of the energetics of a limited atmospheric volume that encompasses the cyclone. The validity of this hypothesis depends upon the extent to which:

1) Energy processes can be defined in a limited region of the atmosphere,

2) The variability of the energy processes can be specified in both time and space.

3) Boundary fluxes of energy can be determined.

4) The interaction of the cyclone with its environment can be determined.

The method that was used to study the energy budget of extratropical disturbances in the present research represents an extension of previous investigations in several respects. First, all the terms of the energy budget equations were considered,

including boundary fluxes of energy that were ignored in most previous studies. Second, objectively analyzed data were used in the evaluation of the various terms of the energy budget equations. Third, the energy budget equations were evaluated throughout the spatial and temporal extent of the cyclone. Results of previous studies were presented in terms of averages, thus providing no information on the variation of the energy processes in time and space. Finally, the interaction of the cyclone with the larger scales of motion is evaluated in a unique manner. While approaches other than the one presented in this paper certainly are feasible, this approach has the advantage of describing the energy budget in terms of the basic physical processes responsible for the energy transformations.

b. Related studies

The first description of a possible means of generating atmospheric motions is credited to Margules (Hess, 1959). He considered two adjacent air masses of different density that were allowed to adjust to a statically stable density stratification which was invariant in the horizontal direction - often referred to as the reference state. During this readjustment, potential energy is converted into kinetic energy. Margules' computations showed that the wind speed generated by this process is comparable to that observed in the atmosphere.

Margules' results, however, apply only to closed atmospheric systems, i.e., systems that include the entire atmosphere. Spar (1950), in a study of energy conversions in a developing cyclone, demonstrated that increases in the kinetic energy of open systems are not necessarily accompanied by decreases in potential energy, as Margules' theory predicts. This is because the boundary fluxes of energy are important in open systems and must be included in the energy budget. An extensive treatment of the role of boundary conditions in open systems has been given by Miller (1950; 1951) and Van Mieghem (1951). It has become clear, however, that the rising of warm air accompanied by the sinking of cold air, as described by Margules, is one of the most important mechanisms responsible for the generation of kinetic energy in a developing cyclone. Margules also initiated the concept of available potential energy, which is defined to be the difference between existing total potential energy (internal + gravitational potential) and the total potential energy that would exist after the entire atmosphere undergoes an isentropic redistribution of mass to the reference state.

With the definition supplied by Margules, Lorentz (1955) developed an approximate expression for the generation of available potential energy. The definition of available potential energy, however, is based on the redistribution of mass of the entire atmosphere toward the reference state, and, until recently,

investigators have found it impossible to apply rigorously the available potential energy concept to a limited region of the atmosphere. This task has been accomplished by Johnson (1970) who has succeeded in prescribing an exact mathematical theory for available potential energy of open systems. Diagnostic studies of energy conversions in developing cyclones based on the theory provided by Johnson should prove helpful in understanding the relationships between energy conversions and cyclogenesis. The concept of available potential energy is useful because it isolates that portion of the total potential energy which is available for conversion to kinetic energy. On the other hand, there is no assurance that all of this energy will in fact be converted, and some controversy exists over what constitutes a realistic state.

Two additional sources for the supply of kinetic energy found in extratropical disturbances were presented in classic papers by Charney (1947) and Kuo (1949). Charney investigated a baroclinic atmosphere and found that the unstable growth of the perturbation in a baroclinic atmosphere results from a conversion of potential energy into kinetic energy. The instability is related to vertical wind shear of the basic current, temperature lapse rate, latitude, and wave length. In an extension of this work, Thompson (1961) has shown that the increase in the kinetic energy of the perturbation is maximized when the thermal wave lags the pressure wave by 90 deg.

Kuo investigated a barotropic atmosphere and found that perturbations in the basic flow will grow when a critical horizontal shear exists. The kinetic energy of the perturbation is increased at the expense of kinetic energy of the basic current. This process represents a transfer of existing kinetic energy from one state to another rather than a conversion of energy from one form to another.

Although the theories of Kuo and Charney appear conflicting, in reality both mechanisms are important and probably occur simultaneously during cyclone development. The relative importance of the two mechanisms is uncertain; although, in a study of one particular cyclone (Johnson, 1970), it was found that two-thirds of the kinetic energy was supplied by the conversions from potential energy and one-third by the kinetic energy of the basic flow.

Since the appearance of these classic papers, innumerable articles treating various aspects of energy transformations have appeared in the literature. These studies can be divided conveniently into two categories. The first category is concerned with average conditions over a long period of time and over a large portion of Earth's surface. This type of study is useful for a better understanding of the general circulation. A summary of a significant number of these articles and the results has been presented by Oort (1964).

The second class of studies deals with kinetic energy generation within individual synoptic systems. The work by Spar (1950) that has already been mentioned is one example. Other notable examples are Palmén (1958), Palmén and Holopainen (1962), Danard (1964), and Eddy (1965). In all of these studies, except for the one by Spar, the term $-\int_V \omega \alpha \, dV''$ has been used to represent the conversion rate between available potential energy and kinetic energy. In the above integral, ω is the vertical velocity in pressure coordinates, α is specific volume, V is the volume over which the integration is performed, and V'' is a dummy variable of integration corresponding to V. When warm air is rising and cold air is sinking, the term $-\int_V \omega \alpha \, dV''$ will be positive, indicating an increase in kinetic energy (White and Saltzman, 1956). However, because of the presence of boundary fluxes of energy, there is no assurance that this term represents the correct value for local conversion rates in open systems (Sechrist and Dutton, 1970; Smith and Horn, 1969). This point will be clarified in a later discussion.

Through the use of the $\omega\alpha$-technique, Palmén (1958) investigated the development of hurricane Hazel into an extratropical cyclone, and found that the conversion rate amounted to 51 watts m^{-2} during the period of strongest development. In similar studies, but for separate synoptic cases, Palmén and Holopainen (1962) computed the conversion rate to be 21 watts m^{-2}; Danard (1964) found a value of 16 watts m^{-2}; and Eddy (1965) found that the most

intense conversion rate, 10 watts m^{-2}, occurred in the middle troposphere ahead of the storm and during the initial development.

If the case involving hurricane Hazel is disregarded, the conversion rates described above are in general agreement. The development of hurricane Hazel into an extratropical cyclone was an unusual event, and cannot be compared with typical extratropical cyclone development.

A unique approach to the study of energy conversions in individual cyclones was developed by Sechrist and Dutton (1970). They considered volumes that moved isentropically with the wind, and thus were able to eliminate boundary conditions and make more precise measurements of the rates of kinetic energy conversion within the volume. In addition, they were able to deduce the geographical sources of the kinetic energy, something not previously possible. Since their results were based on the study of one cyclone, no general conclusions can be made. This approach is promising, but is applicable only when diabatic effects are at a minimum.

After the development of the baroclinic instability theory by Charney, the popular opinion evolved that the extratropical cyclone was maintained against frictional dissipation by the release of this baroclinic instability, and diabatic effects were considered to be minor. Petterssen (1956), however, stressed the physical significance of geographical heat sources and sinks in intensifying

cyclonic or anticyclonic circulations. Further work by Palmén (1958), Danard (1964; 1966), Dutton and Johnson (1967), Palmén and Newton (1969), Johnson (1970), and Bullock and Johnson (1971) has shown that diabatic effects, especially release of latent heat, are indeed important and can be sufficient to offset a major portion of the frictional dissipation of the storm. In fact, it appears that during certain stages of its life cycle, the storm is self-sustaining because of the energy generated by diabatic heating.

From the preceeding discussion, it is evident that much remains to be learned about the energy-cyclogenesis process. While many investigators have attacked various aspects of the problem, a complete description of the energy processes that are active during the various stages of cyclone development is lacking in the meteorological literature. The present research was undertaken in an attempt to fill this void.

c. Objectives

The objective of the present research was to examine the energy budget related to cyclogenesis in the eastern United States, and to establish the relative importance of the various energy processes. In order to accomplish this objective it was necessary to:

1) Develop energy budget equations suitable for a study of this nature.

2) Develop techniques for evaluation of the various terms in the energy budget equations using actual data.

3) Develop a means to display the results of the numerical computations so that energy processes could be related to cyclogenesis.

The details of how these steps were carried out will be discussed fully in the remainder of this paper. At this point it suffices to say that primary consideration was given to developing equations that employ a minimum number of assumptions and that simulate as realistically as possible conditions that occur in the atmosphere. The energy budget equations that were used in the present research were patterned after the ones suggested by Smith (1970). Also, the computational scheme used to evaluate the terms in energy budget equations was designed so that it would incorporate all of the resolution contained in the rawinsonde observations over the eastern United States.

2. THEORETICAL DEVELOPMENT

When the energy equations are applied to global atmospheric processes, the resulting expressions are somewhat simplified because there are no boundary integrals. This is because an integral of the form $\int_V \nabla \cdot A \, dV''$ vanishes when the volume over which the integration takes place encloses the entire atmosphere.

As shown by Wiin-Nielsen (1968), the following relation holds in this situation:

$$\frac{d}{dt}\int_{V^*} b\rho \, dV'' = \int_{V^*} \frac{\partial}{\partial t}(b\rho)\, dV'' = \int_{V^*} \frac{db}{dt}\rho \, dV''. \qquad (1)$$

Here b is any arbitrary scalar defined in the atmosphere, ρ is the density, and V* is the volume that encloses the entire atmosphere. If, however, one considers a volume (V) extending over a limited region of the atmosphere, (1) no longer holds and the following expression must be used:

$$\int_V \frac{\partial}{\partial t}(b\rho)\, dV'' = \int_V \rho \frac{db}{dt}\, dV'' - \int_V \nabla \cdot (\rho b \mathbf{V})\, dV''. \qquad (2)$$

In the above expression $\mathbf{V}$ is the three-dimensional wind vector, ∇ is the three-dimensional del operator, and V is assumed to be independent of time.

The internal, gravitational potential, and kinetic energies for an atmospheric volume, V, are given by

$$I = \int_V c_v \rho T \, dV'', \tag{3}$$

$$P = \int_V g \rho z \, dV'', \tag{4}$$

and

$$K = \int_V \rho \frac{\mathbf{V} \cdot \mathbf{V}}{2} \, dV'', \tag{5}$$

where ρ is the density, C_v is specific heat at constant volume, $g = 980$ cm sec^{-2}, and T is the virtual temperature.

When (2) is applied to (3), the result for the time rate-of-change of internal energy is

$$\frac{\partial I}{\partial t} = \int_V c_v \rho \frac{dT}{dt} \, dV'' - \int_V \nabla \cdot (\rho c_v T \mathbf{V}) \, dV''. \tag{6}$$

An expression for C_v dT/dt can be obtained by combining the thermodynamic equation with the continuity equation to produce

$$c_v \frac{dT}{dt} = \frac{dH}{dt} - \frac{p}{\rho} \nabla \cdot \mathbf{V}, \tag{7}$$

where dH/dt is the diabatic heating per unit mass, and p is pressure. Upon substitution of (7) into (6), we have

$$\frac{\partial I}{\partial t} = \int_V \rho \frac{dH}{dt} dV^* - \int_V p \nabla \cdot \mathbf{V} dV^* - \int_V \nabla \cdot (\rho C_v T \mathbf{V}) dV^*. \tag{8}$$

In a similar manner when (2) is applied to (4), the following equation results,

$$\frac{\partial P}{\partial t} = \int_V g \rho w dV^* - \int_V \nabla \cdot (g \rho z \mathbf{V}) dV^*, \tag{9}$$

where w = dz/dt is the vertical component of $\mathbf{V}$.

Finally, when (2) is applied to (5), we have

$$\frac{\partial K}{\partial t} = \int_V \rho \frac{d}{dt}\left(\frac{\mathbf{V}\cdot\mathbf{V}}{2}\right) dV^* - \int_V \nabla \cdot \left(\rho \frac{\mathbf{V}\cdot\mathbf{V}}{2} \mathbf{V}\right) dV^*, \tag{10}$$

which may be rewritten by substitution of the vector equation of motion to produce,

$$\begin{aligned} \frac{\partial K}{\partial t} = & -\int_V \mathbf{V} \cdot \nabla p \, dV^* - \int_V \rho g w dV^* \\ & + \int_V \mathbf{V} \cdot \mathbf{F} dV^* - \int_V \nabla \cdot \left(\rho \frac{\mathbf{V}\cdot\mathbf{V}}{2} \mathbf{V}\right) dV^*, \end{aligned} \tag{11}$$

where $\mathbf{F}$ is the three-dimensional frictional force.

As a matter of interest, the corresponding expressions for the entire atmosphere, as developed by Wiin-Nielsen (1968) are,

$$\frac{dI}{dt} = \int_{V^*} \rho \frac{dH}{dt} dV'' - \int_{V^*} p \nabla \cdot \mathbf{V} dV'', \tag{12}$$

$$\frac{dP}{dt} = \int_{V^*} \rho g w \, dV'', \tag{13}$$

and

$$\frac{dK}{dt} = -\int_{V^*} \mathbf{V} \cdot \nabla p \, dV'' - \int_{V^*} \rho g w \, dV'' + \int_{V^*} \mathbf{V} \cdot \mathbf{F} \, dV''. \tag{14}$$

These expressions are obviously simpler than (8), (9), and (11) because of the absence of boundary integrals.

Equations (8), (9), and (11) are the ones suggested by Smith (1970) and were the basis for the present research. The advantage of these equations is that they are derived from the thermodynamic equation and the equations of motion, and the individual terms should represent the basic physical processes that cause changes in I, P, and K within a specified closed volume. Before they are used in practice, however, it is necessary to make some modifications.

The first modification that must be made is to apply the hydrostatic approximation. This is necessary simply because the hydrostatic approximation is already incorporated in the rawinsonde

observations that are used to evaluate the various terms in (8), (9), and (11).

When the hydrostatic approximation is invoked, the vertical component of K, $\int_V \rho \frac{w^2}{2} dV''$, becomes invariant, and the expressions corresponding to (8), (9), and (11) become

$$\frac{\partial I}{\partial t} = \int_V \rho \frac{dH}{dt} dV'' - \int_V p \nabla_2 \cdot \mathbf{V}_2 \, dV''$$

$$- \int_V q \rho w_R dV'' - \int_V \nabla \cdot (\rho c_v T \mathbf{V}) dV'', \tag{15}$$

$$\frac{\partial P}{\partial t} = \int_V \rho g w_R dV'' - \int_V \nabla \cdot (\rho g z \mathbf{V}) dV'', \tag{16}$$

and

$$\frac{\partial K_h}{\partial t} = -\int_V \mathbf{V}_2 \cdot \nabla_2 p dV'' + \int_V \mathbf{V}_2 \cdot \mathbf{F} dV'' - \int_V \nabla \cdot \left(\rho \frac{\mathbf{V}_2 \cdot \mathbf{V}_2}{2} \mathbf{V}\right) dV'', \tag{17}$$

where

$$K_h = \int_V \rho \frac{\mathbf{V}_2 \cdot \mathbf{V}_2}{2} dV'' \tag{18}$$

is the horizontal component of K.

Suitable justification for neglecting the vertical portion of K has been presented by Wiin-Nielsen (1968) and Smith (1970).

As pointed out by Richardson (1922), the vertical velocity is no longer a free variable (i.e., one that cannot be derived from basic parameters) in a hydrostatic atmosphere. The symbol w_R is used instead of w for vertical velocity in (15) and (16) to keep this distinction clear.

The differences between a hydrostatic atmosphere and a non-hydrostatic atmosphere become clear when equations (12), (13), and (14) are written in symbolic form following the notation of Wiin-Nielsen (1968). First, for the non-hydrostatic case,

$$\frac{dI}{dt} = G(I) - C(I,K), \tag{19}$$

$$\frac{dP}{dt} = C(K,P), \tag{20}$$

and

$$\frac{dK}{dt} = C(I,K) - C(K,P) - D(K), \tag{21}$$

and, for the hydrostatic case,

$$\frac{dI}{dt} = G(I) - C(I,K_h) - C(I,P), \tag{22}$$

$$\frac{dP}{dt} = C(I,P), \tag{23}$$

and

$$\frac{dK_h}{dt} = C(I,K_h) - D(K_h). \tag{24}$$

In (19) to (24), G(I) refers to generation of internal energy by diabatic processes, C(A,B) refers to a conversion of energy from form A to form B, and D is dissipation. In (20) and (21), the term C(K,P) appears with opposite signs, which means that in a non-hydrostatic atmosphere the kinetic energy may be influenced directly by changes in potential energy. On the other hand, this direct relationship between kinetic and potential energy does not exist in a hydrostatic atmosphere, as can be seen by an examination of (23) and (24). This is because in the hydrostatic atmosphere the potential and internal energies must remain in a constant ratio, as shown by Petterssen (1956); i.e.,

$$P = \frac{R}{C_v} I. \tag{25}$$

Although the atmosphere is never in exact hydrostatic balance, the energetics of the real atmosphere are effectively equivalent to

the energetics of a hydrostatic atmosphere. This is true because the time required for hydrostatic adjustment is small compared to the time scales of the large organized motions (Johnson, 1970).

The interpretation of the terms in (19) to (24) has been given by Wiin-Nielsen (1968). However, Lettau (1954) shows that simple mathematical manipulation can produce several different conversion terms in an open system. Note that the appearance of the terms C(K,P) in (20) and (21) with opposite signs, a necessary condition for an energy conversion process, is possible only because, for a volume enclosing the entire atmosphere,

$$\int_{V^*} p \nabla \cdot \mathbf{V} \, dV'' = -\int_{V^*} \mathbf{V} \cdot \nabla p \, dV''. \tag{26}$$

However, for a limited volume, the following equation holds,

$$\int_{V} p \nabla \cdot \mathbf{V} \, dV'' + \int_{V} \mathbf{V} \cdot \nabla p \, dV'' = \int_{V} \nabla \cdot p \mathbf{V} \, dV''. \tag{27}$$

Smith, citing work by Pfeffer (1957) states that unless the boundary transport term, $\int_{V} \nabla \cdot p \mathbf{V} \, dV''$, is identically zero, neither of the two terms on the left-hand side of (27) can be regarded as specifying the rate of conversion between I and K. Smith overcomes this difficulty by writing

$$\int_{V^*} \nabla \cdot p \mathbf{V} \, dV'' = 0 = \int_{V} \nabla \cdot p \mathbf{V} \, dV'' + \int_{V'} \nabla \cdot p \mathbf{V} \, dV'', \tag{28}$$

where V* and V are as defined previously, and V' is the atmospheric volume surrounding V, i.e.,

$$V' = V^* - V. \tag{29}$$

Thus, the boundary work within V is balanced outside of V by that done within V'. This permits the interpretation of the term, $\int_V \nabla \cdot p\mathbf{V}\, dV^*$, in (27) as a transformation of internal energy within V to internal energy in the surrounding volume, V'. The obvious advantage of this manipulation is that it permits the study of the interaction of V and the surrounding atmosphere. When (27) is substituted into (8) along with the hydrostatic approximation, the following expression results:

$$\frac{\partial I}{\partial t} = \int_V \rho \frac{dH}{dt}\, dV'' + \int_V \mathbf{V}_2 \cdot \nabla_2 p\, dV'' - \int_V g\rho w_R\, dV'' - \int_V \nabla \cdot p\mathbf{V}\, dV'' - \int_V \nabla \cdot (\rho c_v T \mathbf{V})\, dV''. \tag{30}$$

Finally, by defining $\Pi = P + I$, we can combine (9) and (30) to form

$$\frac{\partial \Pi}{\partial t} = \int_V \rho \frac{dH}{dt} dV'' + \int_V \mathbf{V}_2 \cdot \nabla_2 p\, dV'' - \int_V \nabla \cdot p\mathbf{V}\, dV'' - \int_V \nabla \cdot (\rho c_p T \mathbf{V})\, dV'', \tag{31}$$

where C_p is the specific heat at constant pressure.

For computational purposes it is convenient to express (3), (4), and (5) in an x,y,p,t-system, since pressure usually is used as the vertical coordinate rather than height.

We can write the total potential energy (π), by assuming hydrostatic equilibrium and using (25) as

$$\pi = \frac{c_p}{g} \int_A \int_{p_2}^{p_1} T \, dp \, dA'' \, . \tag{32}$$

In a similar manner, the horizontal component of K becomes

$$K_h = \frac{1}{g} \int_A \int_{p_2}^{p_1} \frac{V_2 \cdot V_2}{2} \, dp \, dA'' \, , \tag{33}$$

where A is the horizontal cross-sectional area of V, A'' is a dummy variable of integration corresponding to A, and p_1 and p_2 are the pressures at the bottom and top of an unspecified layer in the atmosphere.

Equations (17) and (31) can be transformed to an x,y,p,t coordinate system through the use of the following relationships (Thompson, 1961),

$$\left(\frac{\partial \Phi}{\partial x}\right)_z = \left(\frac{\partial \Phi}{\partial x}\right)_p + \frac{\partial \Phi}{\partial p}\left(\frac{\partial p}{\partial x}\right)_z \, , \tag{34a}$$

$$\left(\frac{\partial \Phi}{\partial y}\right)_z = \left(\frac{\partial \Phi}{\partial y}\right)_p + \frac{\partial \Phi}{\partial p}\left(\frac{\partial p}{\partial y}\right)_z \, , \tag{34b}$$

$$\frac{\partial \Phi}{\partial z} = \frac{\partial \Phi}{\partial p}\frac{\partial p}{\partial z} , \tag{34c}$$

and

$$\frac{1}{\rho}\nabla p = g\nabla_p z , \tag{34d}$$

where Φ is any scalar quantity. Upon substitution of (34) into (17) and (31), the final energy budget equations become,

$$\frac{\partial \pi}{\partial t} = \frac{1}{g}\int_A\int_{p_2}^{p_1}\frac{dH}{dt}\,dp\,dA'' + \int_A\int_{p_2}^{p_1} V_2\cdot\nabla_p z\,dp\,dA''$$

$$-\frac{R}{g}\int_A\int_{p_2}^{p_1}\left[\nabla_p\cdot T V_2 + \frac{\partial}{\partial p}(T\omega)\right]dp\,dA''$$

$$-\frac{c_p}{g}\int_A\int_{p_2}^{p_1}\left[\nabla_p\cdot T V_2 + \frac{\partial}{\partial p}(T\omega)\right]dp\,dA'', \tag{35}$$

and

$$\frac{\partial K_h}{\partial t} = -\int_A \int_{p_2}^{p_1} V_2 \cdot \nabla_p Z \, dp \, dA''$$

$$+ \frac{1}{g} \int_A \int_{p_2}^{p_1} \frac{1}{\rho} V_2 \cdot F \, dp \, dA''$$

$$-\frac{1}{g} \int_A \int_{p_2}^{p_1} \left[\nabla_p \cdot \left(\frac{V_2 \cdot V_2}{2} V_2 \right) + \frac{\partial}{\partial p} \left(\frac{V_2 \cdot V_2}{2} \omega \right) \right] dp \, dA'', \quad (36)$$

where $\omega = dp/dt$.

The interpretation of the terms in (35) and (36) is as follows. The first term on the right-hand side of (35) represents changes in total potential energy caused by diabatic processes. The second term on the right-hand side of (35) represents the rate at which total potential energy is changed due to cross-contour or non-geostrophic flow. This term also appears on the right-hand side of (36), but with an opposite sign, and thus may be regarded as the term that represents conversion between total potential and kinetic energy. The third term on the right-hand side of (35) corresponds to the first term in (29), and as shown previously this term represents the conversion of total potential energy within V to total potential energy in the surrounding atmosphere. The last terms in (35) and (36) represent the flux of total potential and

kinetic energy through the boundaries of V. Finally, the second term on the right-hand side of (36) represents changes in kinetic energy due to frictional forces.

In the remainder of the text, the following symbolic notation will be used when referring to the terms described above:

$G(\pi)$ - Changes in total potential energy due to diabatic processes.

$C(\pi, K_h)$ - Conversion of total potential energy into kinetic energy.

$C(\pi, \pi')$ - Conversion of total potential energy within a volume to potential energy in the surrounding volume.

$H(\pi)$ - Horizontal component of the boundary flux of total potential energy.

$VF(\pi)$ - Vertical component of the boundary flux of total potential energy.

$H(K_h)$ - Horizontal component of the boundary flux of kinetic energy.

$VF(K_h)$ - Vertical component of the boundary flux of kinetic energy.

$D(K_h)$ - Dissipation of kinetic energy.

Equations (35) and (36) are the energy budget equations that were used to investigate the relationships between energy processes and cyclogenesis. The various terms in (35) and (36) were evaluated

with actual rawinsonde observations in a manner that will be explained in the next section.

3. ANALYTICAL PROCEDURES

a. The grid system

Computation of the various terms in the energy budget equations is facilitated if the data points are uniformly distributed in space. Since the rawinsonde observations used in this study are arranged in a random manner, it was desirable to interpolate the observations to equally spaced grid points. The grid system used in this study is shown in Fig. 1.

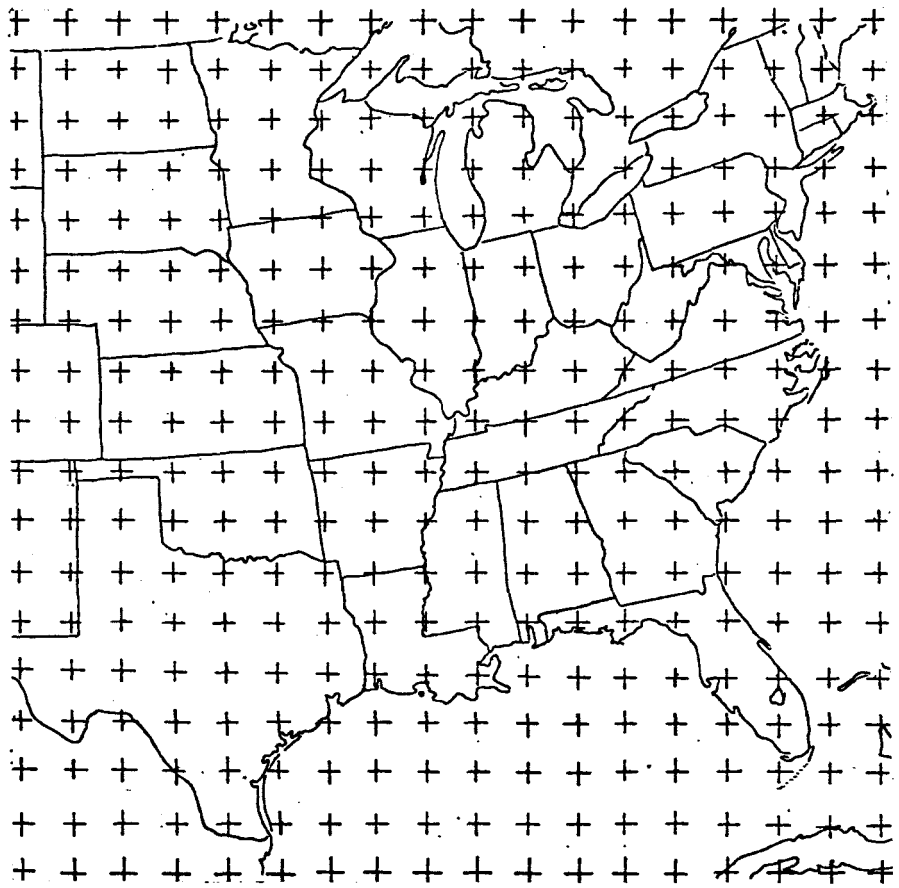

Fig. 1. Grid used for numerical computations.

The grid spacing is ½ in. on a 1:12,500,000 conformal conic projection with true latitudes at 30 and 60 deg N. The conformal conic projection was selected because the map scale factor varies only slightly (0.98 to 1.02) over the area of interest. This slight variation was neglected, and a value of 1.0 was used in this study. The ½-in. grid spacing is convenient also because it enables one to produce printed output from a computer that is the same scale as the 1:12,500,000 conformal conic projection.

The ½-in. spacing of grid points corresponds to a distance of approximately 158 km between grid points. This distance is more than adequate to resolve any of the information contained in the rawinsonde observations. In fact, in a very recent study by Barr et al. (1971), it is shown theoretically that a 169-km grid interval incorporates as much detail as can be justified from the existing rawinsonde network over the United States.

b. Interpolation procedures

The rawinsonde and surface observations were interpolated to the grid using an objective analysis scheme developed by Barnes (1964). This procedure is commonly referred to as successive corrections to a first-guess field. First-guess fields usually are derived from forecast fields, persistence, climatology, or various combinations of the three. Since none of these was available, zero was used as the first guess in this study. This has a certain disadvantage because forecast fields can be used to detect obvious

errors in the data. Since forecast fields were not available, extensive hand checking of the data was required to eliminate errors.

The steps in the analysis procedure are as follows. The observations are scanned in order, and for the k^{th} observation, the error (E^k) between the observation and the first-guess analysis at the observation location is computed. The value of the analysis at the observation location is found by bi-linear interpolation. This error then influences a number of grid points in the vicinity of the observation location with the amount of influence or weight varying with the distance between the grid point and the observation location. The weight (w_{ij}^k) for grid point (i,j) is given by

$$w_{ij}^k = e^{-4r^2/(SR)^2},$$

where r is the distance from the k^{th} observation to the grid point, and SR is the scan radius. A scan radius of 4 grid units was used in this study. Barnes has shown this value to be optimum for the rawinsonde density of the eastern United States. Only the grid points within a distance SR from the observation point are influenced. w_{ij}^k has a value of unity when the grid and observation points coincide, and approaches zero as the distance from the observation point increases.

Any particular grid point may be influenced by several observations, and after all of the observations have been considered, the total correction (c_{ij}) for each grid point is determined by

$$C_{ij} = \sum_{k=1}^{N} E^{k} W_{ij}^{k} \Big/ \sum_{k=1}^{N} W_{ij}^{k} ,$$

where N is the number of observations influencing grid point (i,j). The total corrections are added to the first-guess field to provide a new first-guess field.

The above procedure is repeated until there is close agreement between the observations and the analysis. Barnes has demonstrated mathematically the convergence of this procedure, and shows that the number of iterations for convergence depends on the amount of information contained in the observations. Four iterations were found to be sufficient for the purposes of this study.

The choice of this technique over the more commonly used interpolation procedure of Cressman (1959) was motivated by two factors. The Cressman technique makes use of a decreasing scan radius on each successive iteration, whereas the scan radius is held fixed in the Barnes technique. It can be shown that decreasing the scan radius will result in an amplification of the errors in the observations with each successive iteration. The fixed scan radius eliminates this problem and the errors in analysis due to errors in observations are constant from one iteration to the next. If the Cressman technique is used, extensive smoothing must be employed to eliminate noise introduced by the

errors in the observations. The smoothing in turn destroys some of the circulation centers.

The Barnes technique also provides a superior representation of gradients. The main advantage of the Cressman technique is that it requires fewer computations because, after the first iteration, fewer grid points are influenced by each observation than with the Barnes technique.

c. Description of analyzed fields

Gridded analyses of height, temperature, and wind components were made for the 1000-, 850-, 700-, 500-, 400-, 300-, 200-, and 100-mb levels. The analyses then were interpolated vertically to produce ten levels of information at 1000, 900, 800, 700, 600, 500, 400, 300, 200, and 100 mb. Cubic interpolation was used to arrive at the temperature and wind components at the interpolated levels of 900, 800, and 600 mb. The heights at these levels were computed using the hypsometric equation.

The data used to produce the analyses consisted of 0000 and 1200 GMT rawinsonde and surface observations. Whenever possible, observations outside of the grid were used so that the boundary grid points would be just as reliable as the interior points.

The analyzed fields were smoothed using a nine-point filter with a smoothing weight of 0.5 as described by Shuman (1957). This smoothing filter is defined by

$$\bar{A}_0 = A_0 + \tfrac{1}{2}\nu(1-\nu)(A_1 + A_2 + A_3 + A_4 - 4A_0) + \tfrac{1}{4}\nu^2(A_5 + A_6 + A_7 + A_8 - 4A_0)$$

where A represents the field value at the various points indicated by the subscripts shown in Fig. 2, and ν is the smoothing weight.

6	2	5
3	0	1
7	4	8

Fig. 2. Nine-point smoothing mesh.

Barr et al. (1971) have shown that wave lengths of less than approximately 1700 km cannot be represented by the data from the existing rawinsonde network over the United States. The filter described above retains virtually 100% of the amplitude of wave lengths greater than 1500 km while eliminating the smaller wave lengths that are due to spurious small-scale fluctuations in the observations.

d. Computation of vertical velocities

The choice of a method for the computation of vertical velocities was not easy because none of the known methods yields entirely satisfactory results. The kinematic method was used in this study with the assumption that $\omega = 0$ at p = 1000 mb. This method was chosen because it uses actual winds and involves the least stringent assumptions.

Two other commonly-used methods that were considered are the adiabatic method and the ω-equation method. The adiabatic method was discarded because it produces erroneous results when applied to energy conversions due to the omission of diabatic processes (Wiin-Nielsen, 1964). Solution of the ω-equation requires that ω be specified on the boundaries of the grid, and these boundary values can affect significantly the interior values because the grid used in this study covers a relatively small area. Other methods that use the quasi-geostrophic assumption were not considered because there is a significant difference between energy transformations in an atmosphere that is in geostrophic balance versus one in ageostrophic balance.

e. Determination of the dissipation of kinetic energy

The frictional dissipation in the boundary layer was computed through the use a relationship given by Lettau (1959):

$$D(K_h) = \rho C^2 U_g^3 \cos\gamma \qquad (37)$$

where

$$C = k' \left[\ln \frac{U_g}{z_o f} - 1.865 \right]^{-1},$$

and U_g is the geostrophic wind speed at 1000 mb, γ is the angular departure from the geostrophic wind and shear stress vectors,

k' is the von Karman constant, f is the Coriolis parameter, and Z_0 is the roughness parameter. The values for γ , k', and Z_0 were taken to be 20 deg, 0.4, and 50 cm, respectively. These values have been suggested as representative for the eastern United States by Bullock and Johnson (1971).

The dissipation of kinetic energy in the free atmosphere has been computed by Holopainen (1963), Kung (1966), and others as the residual term in equations similar to (36). However, these computations were averaged over several months, and no estimates of free atmospheric dissipation in individual storms are available. As the results of this study will indicate, it is doubtful whether the various terms in (36) can be computed with sufficient accuracy for a single storm to determine dissipation as the residual term.

An approximate expression for the dissipation term in the free atmosphere has been presented by Palmen and Newton (1969) as

$$D(K_h) = \int_V \rho \mu_h \left[\left(\frac{\partial u}{\partial z} \right)^2 + \left(\frac{\partial v}{\partial z} \right)^2 \right] dV'',$$

where μ_h is a coefficient of lateral mixing. However, μ_h is not known with sufficient accuracy to make the above expression usable.

f. Numerical evaluation of integrals

The integrands on the right-hand side of (32), (33), (35), and (36) were evaluated at each of the levels between 1000 and 100 mb. In general, centered differences were used except for the evaluation of time derivatives where 12-hour backward differences were used. The use of centered differences reduced the original 18 x 18 grid to 16 x 16.

Vertical integrations then were carried out through the use of the trapezoidal rule for the layers 1000-700 mb, 700-400 mb, and 400-100 mb. The partial integrals for the three layers were summed to obtain values for the entire depth 1000-100 mb.

Units of joules m^{-2} were used to express kinetic and total potential energy. Units of watts m^{-2} were used for terms involving conversions of energy. Numerical computations were performed on the IBM 360/65 computer at Texas A&M University.

4. DESCRIPTION OF SYNOPTIC CASES

a. Selection criteria

Examples of cyclone development over the eastern United States are not difficult to find since cyclogenesis is a common occurrence in this area, particularly during the winter months. The primary consideration for the selection of synoptic cases for study was that the various stages of cyclogenesis had to occur while the cyclone was within the confines of the grid shown in Fig. 1 (p. 25). Only cases that occurred within the last 5 years were considered because of availability of data at Texas A&M University.

The two synoptic cases that were chosen now will be discussed briefly. These cases have many similarities, but as will be shown later, the energy processes and the mechanisms responsible for cyclogenesis in the two cases were quite different.

b. Case I: 1-4 November 1966

The first indication of cyclogenesis at the surface occurred at 1200 GMT on 1 November 1966 as a weak wave developed on the frontal system through the Gulf of Mexico (Fig. 3a). The low-pressure center associated with this wave moved northeastward into Florida, and by 0000 GMT on 2 November 1966, a closed circulation was evident at the surface (Fig. 4a). The low center then moved in a north-to-northwestward direction toward the Great Lakes, and rapid deepening occurred until near 1200 GMT on 3 November 1966

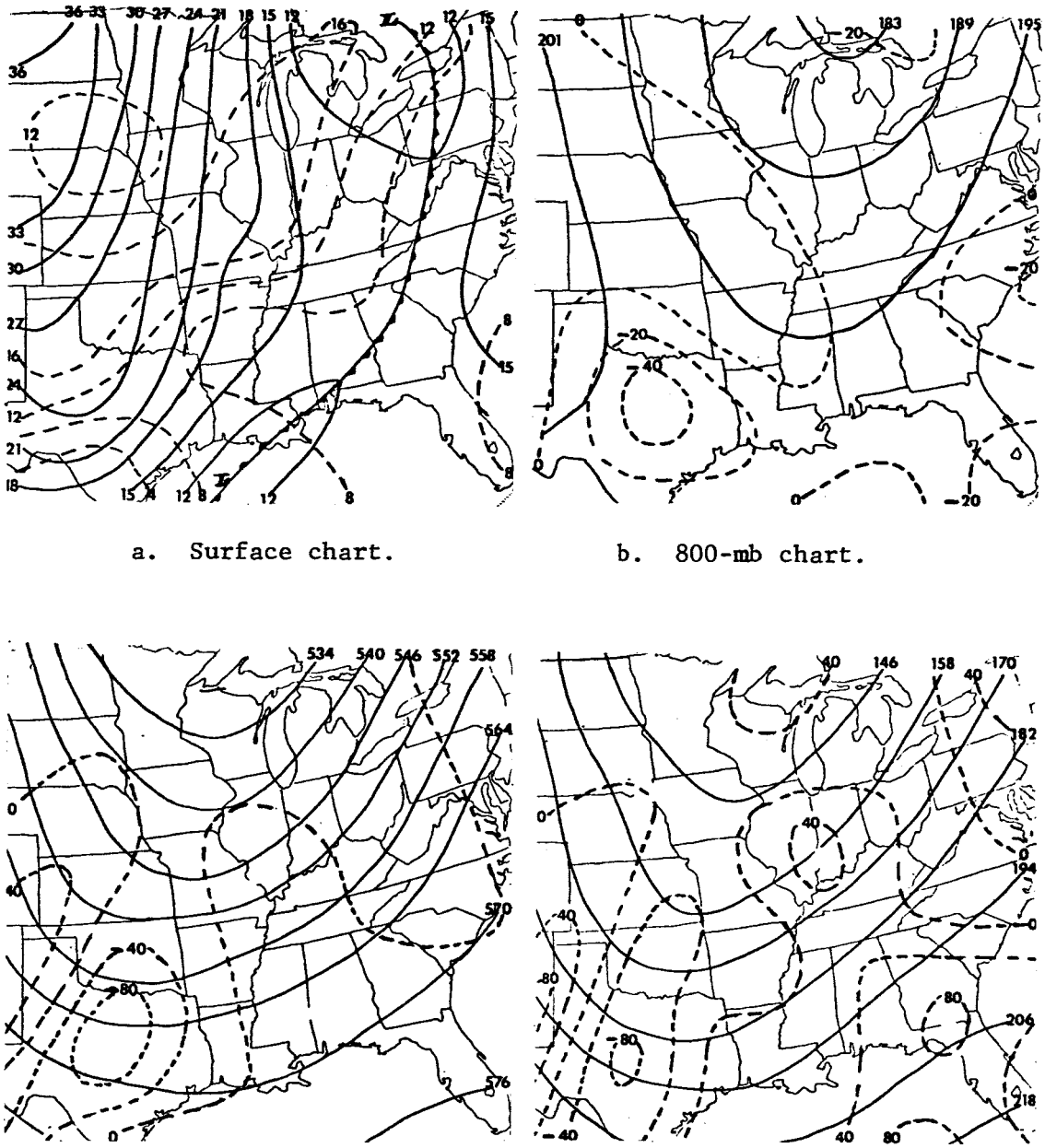

Fig. 3. Synoptic maps for 1200 GMT, 1 November 1966. (Dashed lines on surface map represent 500-mb vorticity (10^{-5} sec^{-1}). Dashed lines on upper-level maps are values of ω (10^{-4} mb sec^{-1}).)

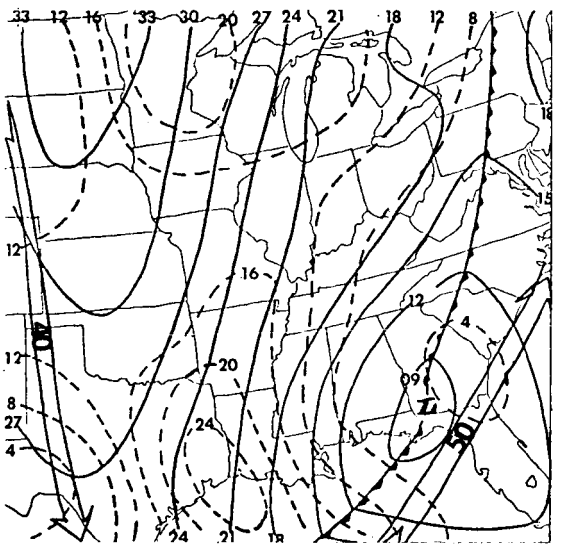

a. Surface chart.

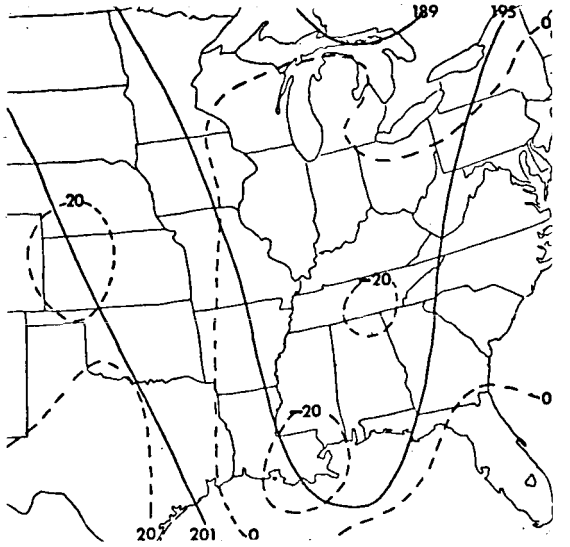

b. 800-mb chart.

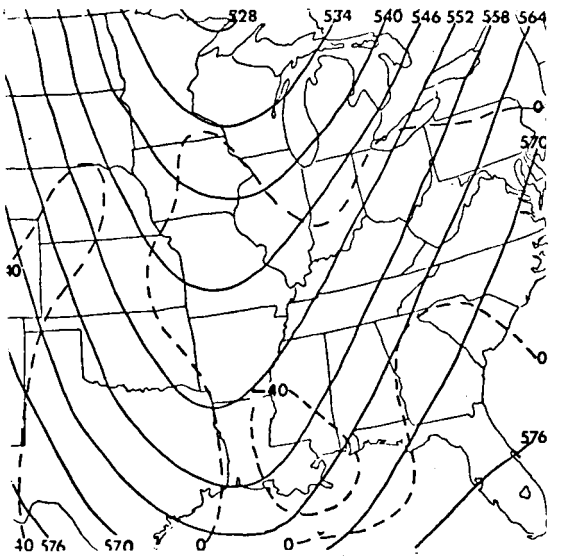

c. 500-mb chart.

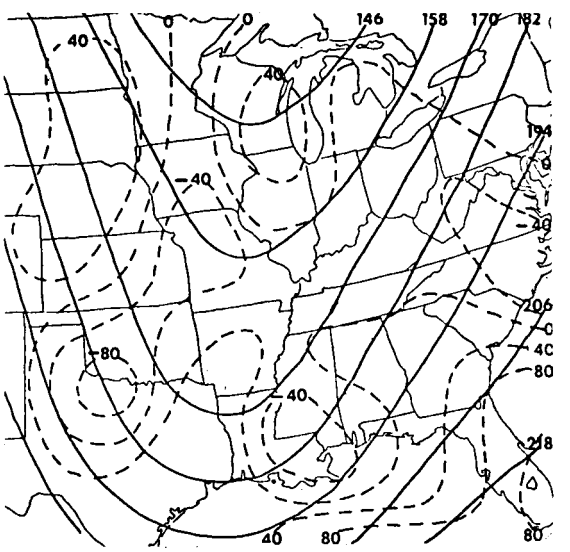

d. 200-mb chart.

Fig. 4. Synoptic maps for 0000 GMT, 2 November 1966. (Dashed lines on surface map represent 500-mb vorticity (10^{-5} sec^{-1}). Dashed lines on upper-level maps are values of ω (10^{-4} mb sec^{-1}).)

(Fig. 6a) at which time the low reached its greatest intensity (see Figs. 5a, 6a, and 7a). By 0000 GMT on 4 November 1966, the low center had moved north of the Great Lakes, and was dissipating slowly (Fig. 8a).

Upper-air charts for selected levels also are shown in Figs. 3 to 8 to present a three-dimensional picture of the atmosphere during the period of cyclogenesis. An intense trough can be noted to the west of the surface low at all levels above the surface during the period when cyclogenesis was occurring. The southern portion of the trough moved eastward and sharpened while the northern portion remained relatively stationary.

The approximate location of the jet stream (the position of the 200-mb maximum winds) is shown on the surface charts in Figs. 3 to 8. Wind speeds in excess of 70 m sec^{-1} can be noted along the east coast of the United States in Fig. 6a. The implications of this jet stream will be discussed later, and evidence will be presented that indicates that this jet stream provided the initial impulse of kinetic energy to the cyclone.

This synoptic case is somewhat unusual because the track of the cyclone is farther west than usual. Normally, in a synoptic situation of this type, intense cyclogenesis will occur off the coast of the Carolinas, and the low center will move northward, remaining just off the east coast of the United States.

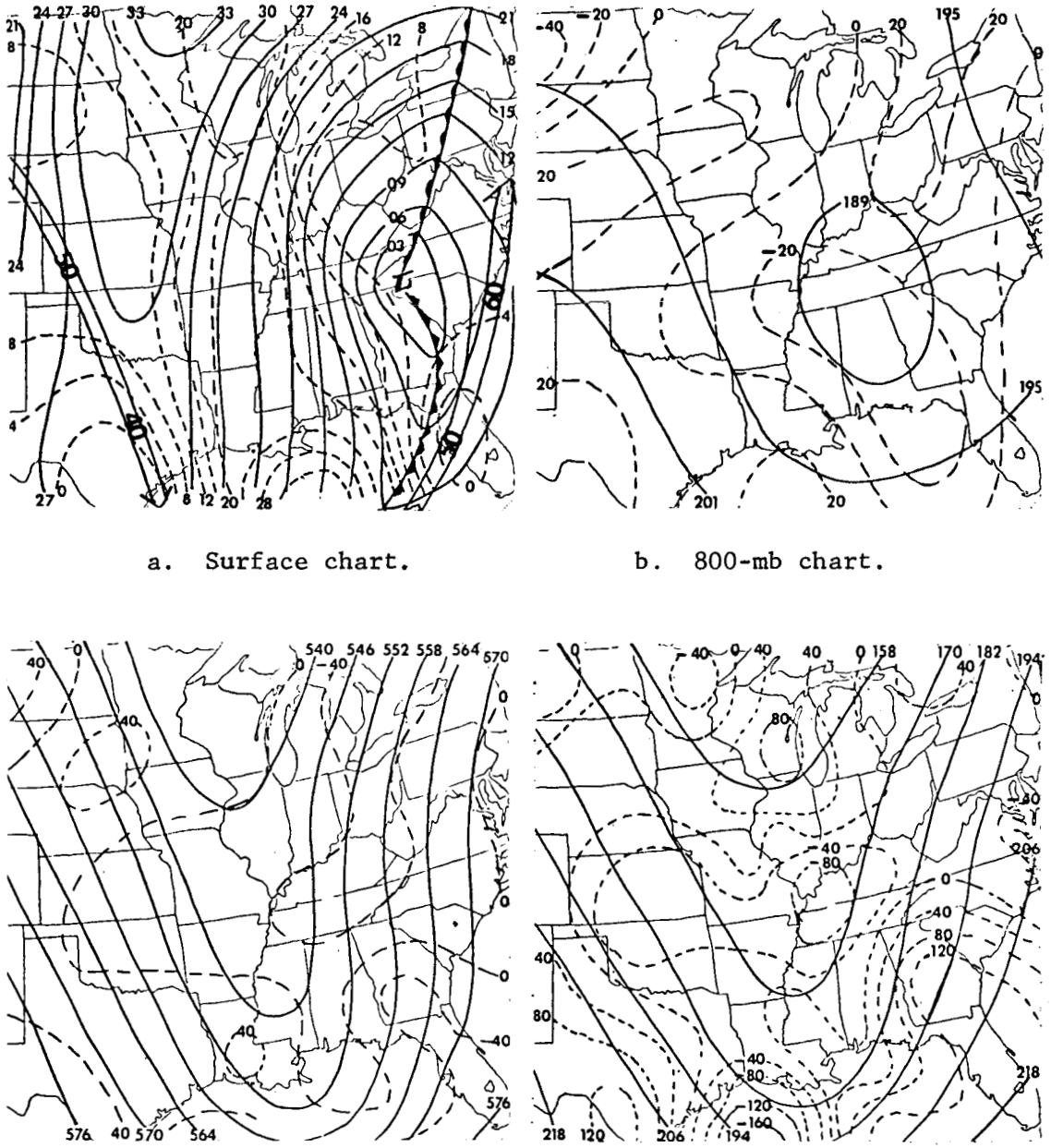

a. Surface chart.

b. 800-mb chart.

c. 500-mb chart.

d. 200-mb chart.

Fig. 5. Synoptic maps for 1200 GMT, 2 November 1966. (Dashed lines on surface map represent 500-mb vorticity (10^{-5} sec^{-1}). Dashed lines on upper-level maps are values of ω (10^{-4} mb sec^{-1}).)

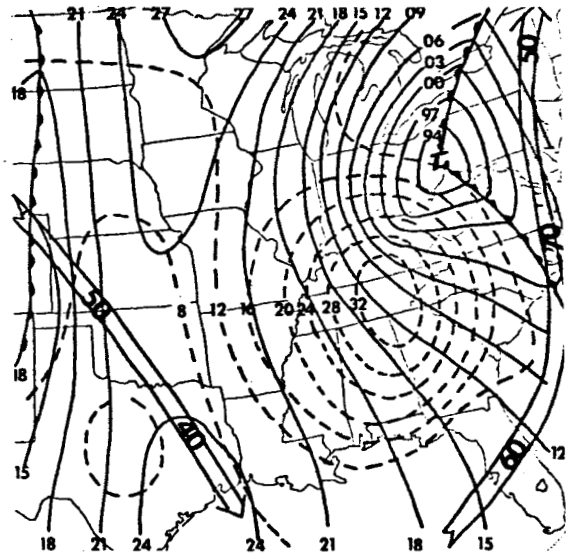

a. Surface chart.

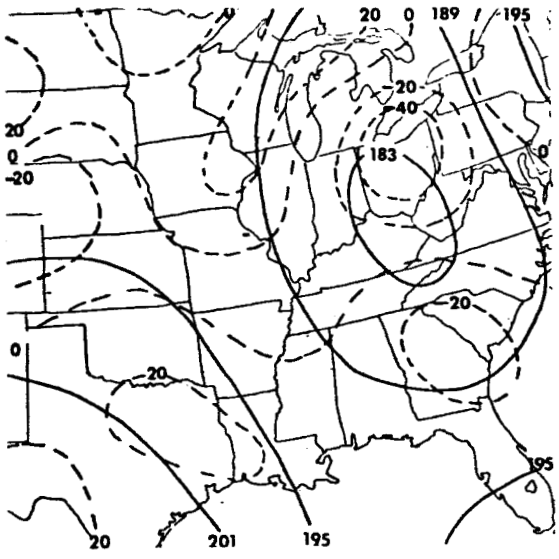

b. 800-mb chart.

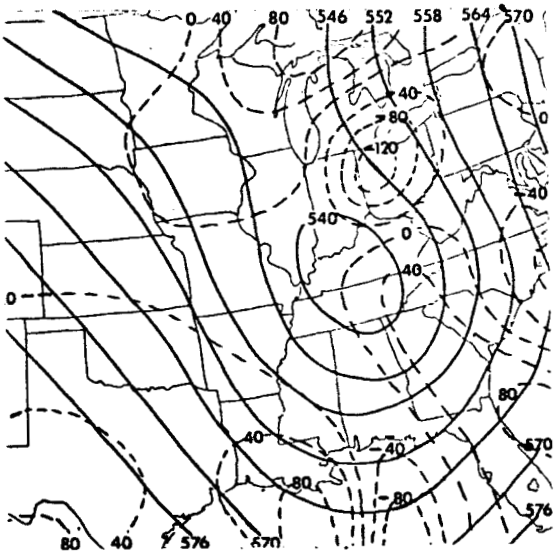

c. 500-mb chart.

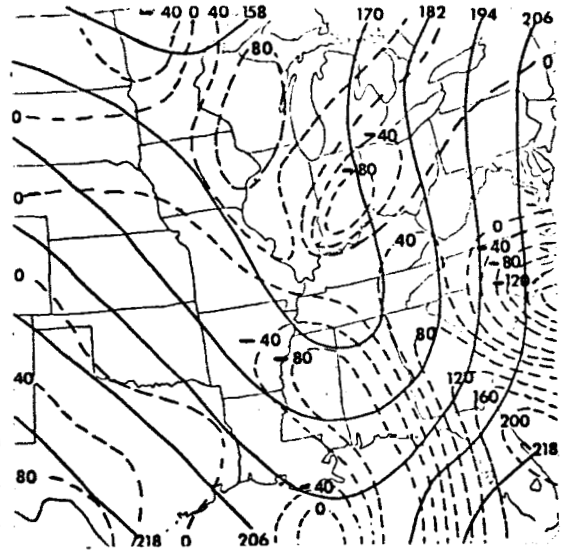

d. 200-mb chart.

Fig. 6. Synoptic maps for 0000 GMT, 3 November 1966. (Dashed lines on surface map represent 500-mb vorticity (10^{-5} sec^{-1}). Dashed lines on upper-level maps are values of ω (10^{-4} mb sec^{-1}).)

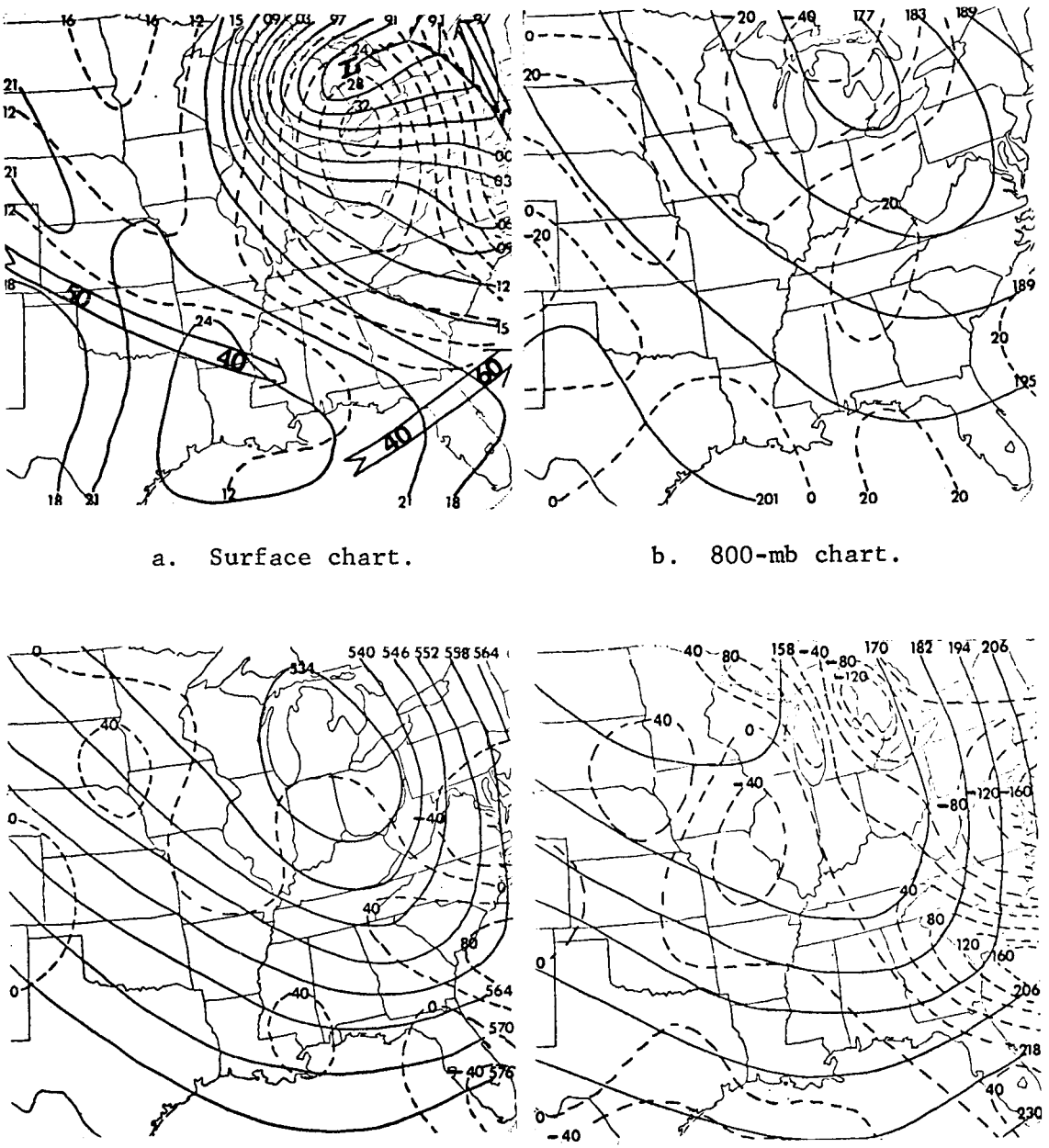

Fig. 7. Synoptic maps for 1200 GMT, 3 November 1966. (Dashed lines on surface map represent 500-mb vorticity (10^{-5} sec^{-1}). Dashed lines on upper-level maps are values of ω (10^{-4} mb sec^{-1}).)

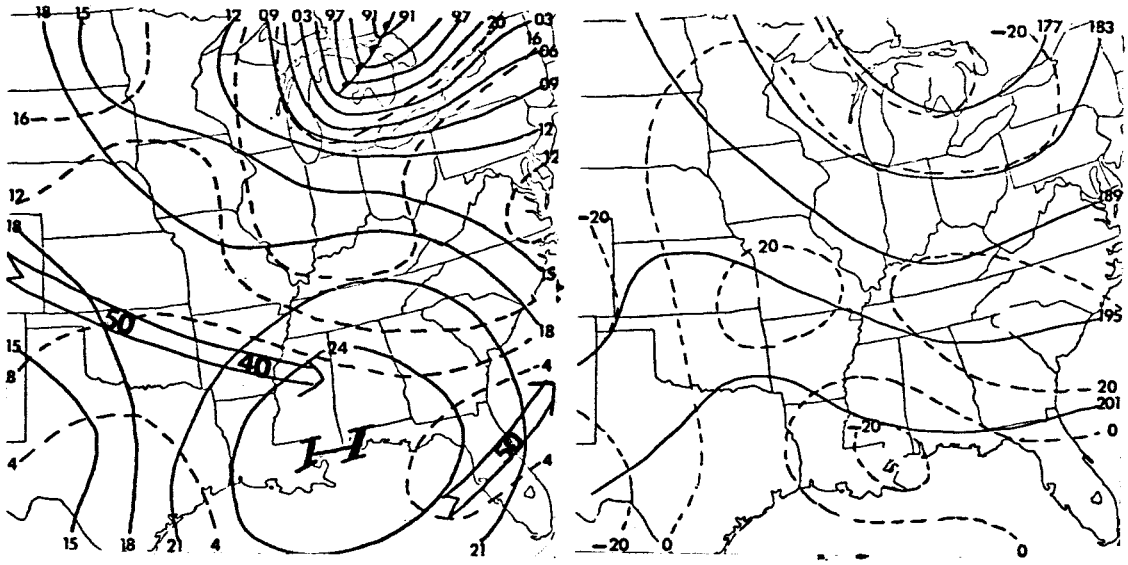

a. Surface chart.

b. 800-mb chart.

c. 500-mb chart.

d. 200-mb chart.

Fig. 8. Synoptic maps for 0000 GMT, 4 November 1966. (Dashed lines on surface map represent 500-mb vorticity (10^{-5} sec^{-1}). Dashed lines on upper-level maps are values of ω (10^{-4} mb sec^{-1}).)

c. Case II: 5-8 December 1969

At the beginning of this period, a weak low-pressure center was evident at the surface in eastern New Mexico (Fig. 9a). The low then moved southeastward into Texas (Figs. 10a and 11a) with little change in intensity. The low center then turned and moved northward (Figs. 12a to 14a) and the circulation around the center intensified considerably. By 1200 GMT, 8 December 1969, the low center had reached Lake Superior, and had entered the dissipation stage (Fig. 15a). The remarkable feature of this low is that the central pressure remained steady at approximately 998 mb throughout the period.

The associated upper-air charts are shown in Figs. 9 to 15. As the low intensified at the surface, the upper-level trough also intensified, and by the end of the period a closed circulation can be noted at all levels (Figs. 14 and 15). This can be contrasted with the first case where this closed circulation existed only in the lower troposphere even when the low had reached its maximum development.

Another interesting feature of this case is the organized patterns of vertical motion that can be seen in Figs. 11 to 13. These patterns were not nearly as evident in the first case. The role of these organized patterns of vertical motion in producing energy transformations and contributing to cyclogenesis will be discussed in detail in the next section.

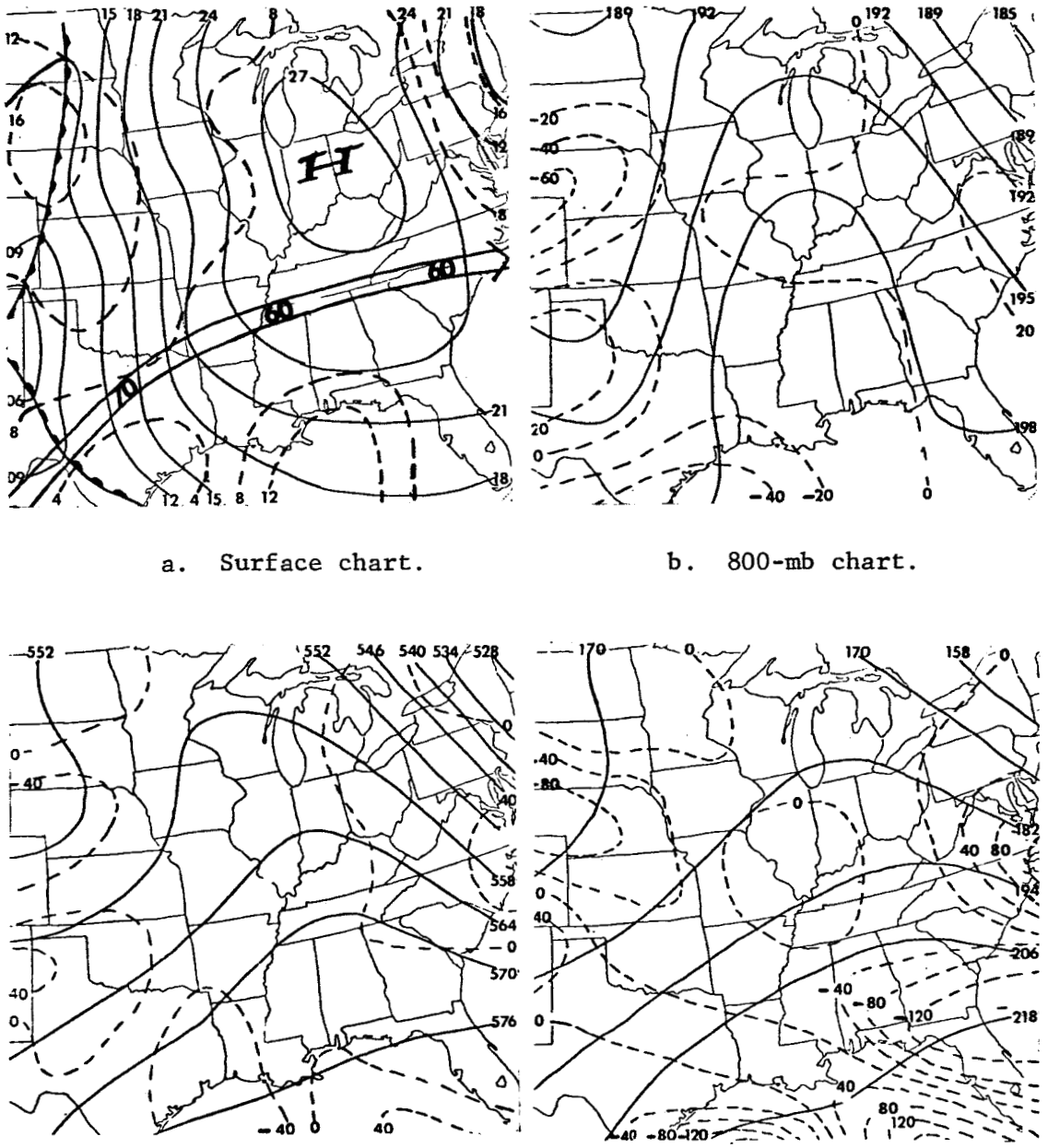

a. Surface chart.

b. 800-mb chart.

c. 500-mb chart.

d. 200-mb chart.

Fig. 9. Synoptic maps for 1200 GMT, 5 December 1969. (Dashed lines on surface map represent 500-mb vorticity (10^{-5} sec^{-1}). Dashed lines on upper-level maps are values of ω (10^{-4} mb sec^{-1}).)

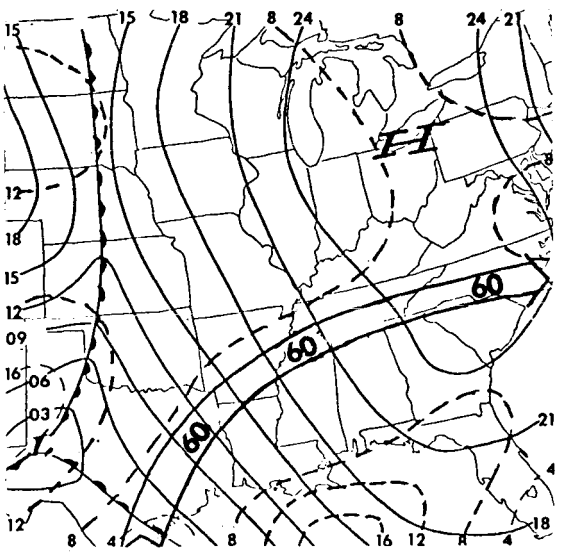

a. Surface chart.

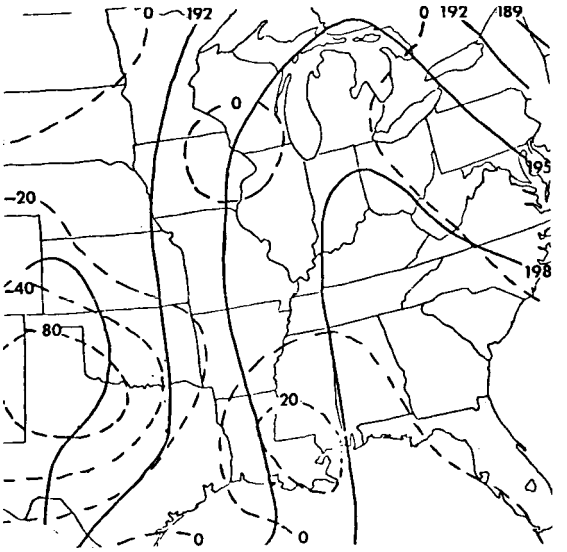

b. 800-mb chart.

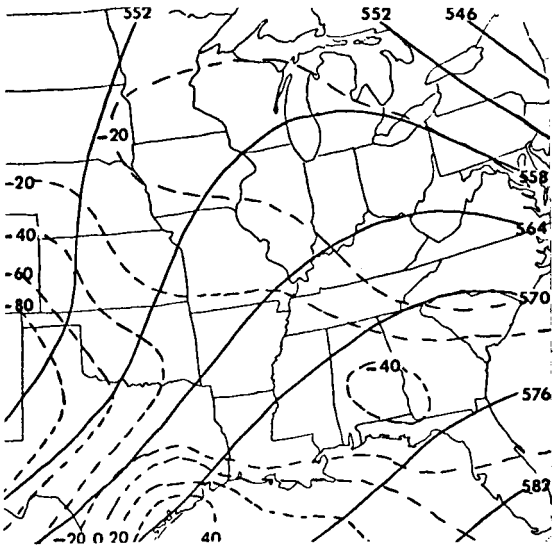

c. 500-mb chart.

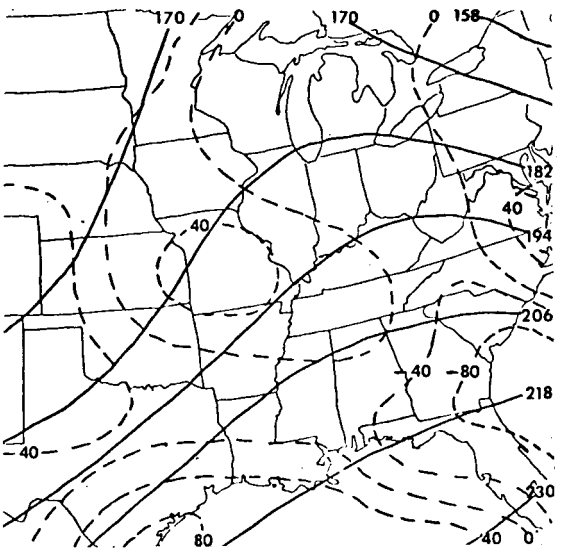

d. 200-mb chart.

Fig. 10. Synoptic maps for 0000 GMT, 6 December 1969. (Dashed lines on surface map represent 500-mb vorticity (10^{-5} sec^{-1}). Dashed lines on upper-level maps are values of ω (10^{-4} mb sec^{-1}).)

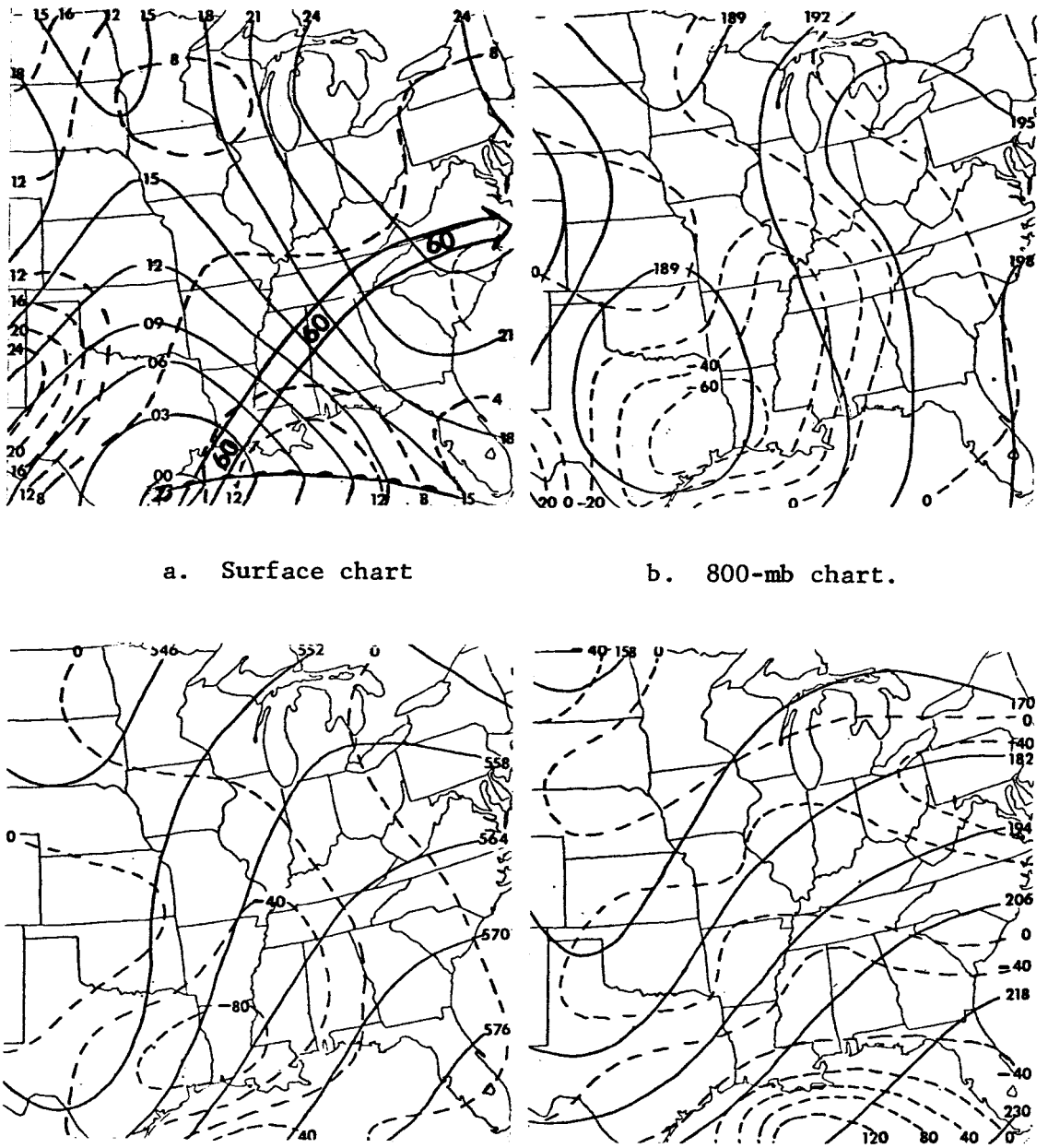

Fig. 11. Synoptic maps for 1200 GMT, 6 December 1969. (Dashed lines on surface map represent 500-mb vorticity (10^{-5} sec^{-1}). Dashed lines on upper-level maps are values of ω (10^{-4} mb sec^{-1}).)

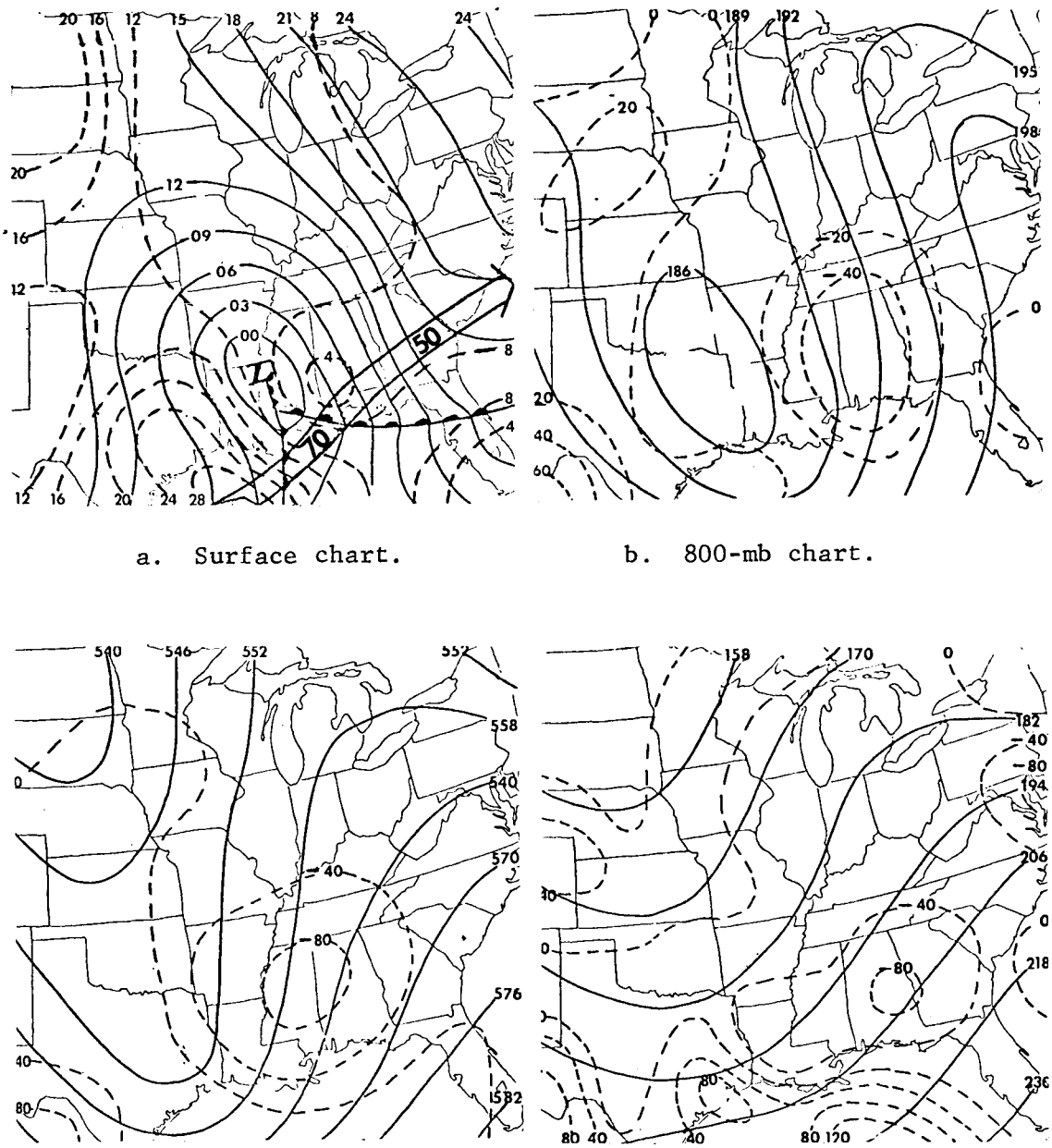

a. Surface chart.

b. 800-mb chart.

c. 500-mb chart.

d. 200-mb chart.

Fig. 12. Synoptic maps for 0000 GMT, 7 December 1969. (Dashed lines on surface map represent 500-mb vorticity (10^{-5} sec^{-1}). Dashed lines on upper-level maps are values of ω (10^{-4} mb sec^{-1}).)

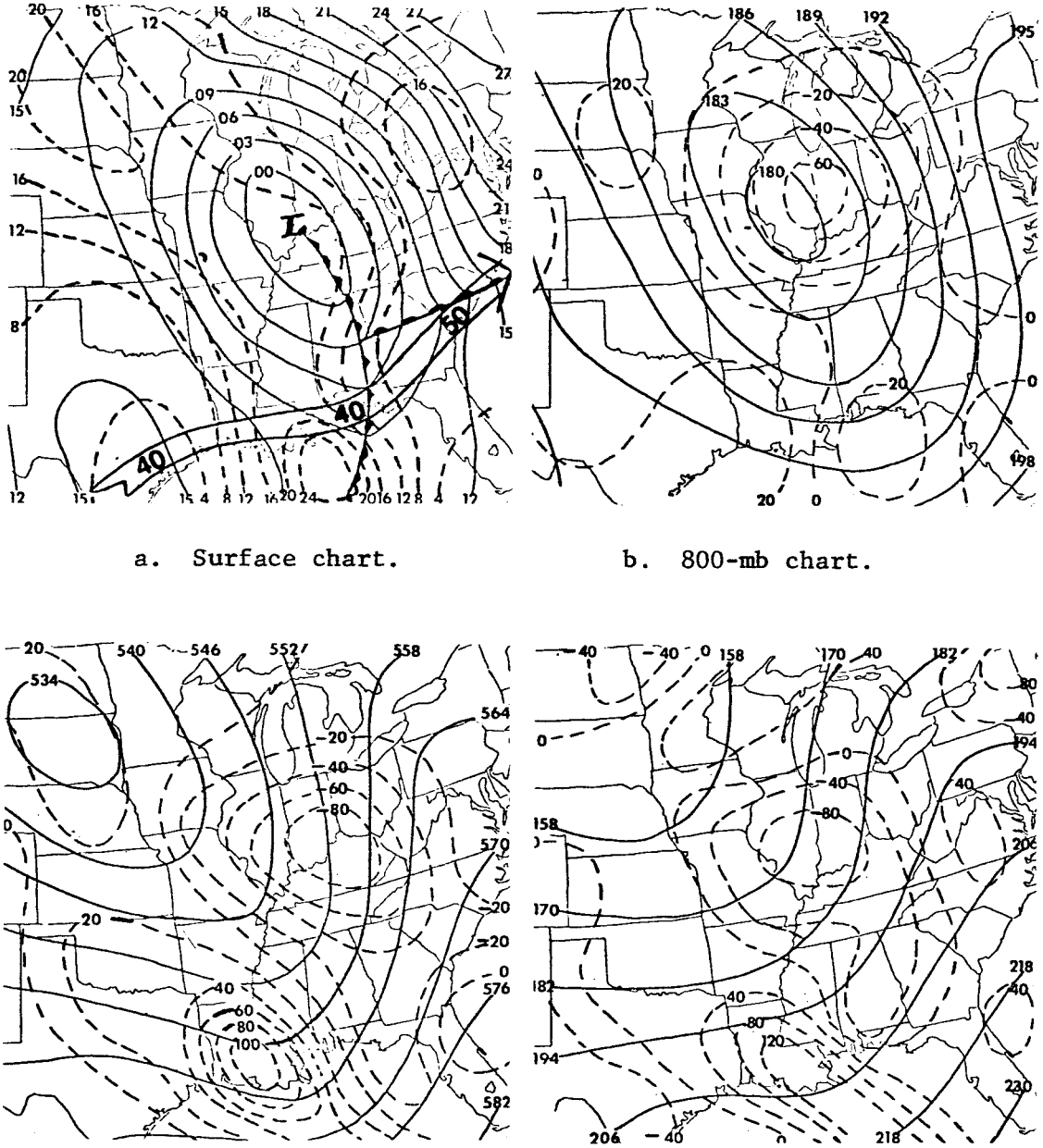

a. Surface chart.

b. 800-mb chart.

c. 500-mb chart.

d. 200-mb chart.

Fig. 13. Synoptic maps for 1200 GMT, 7 December 1969. (Dashed lines on surface map represent 500-mb vorticity (10^{-5} sec^{-1}). Dashed lines on upper-level maps are values of ω (10^{-4} mb sec^{-1}).)

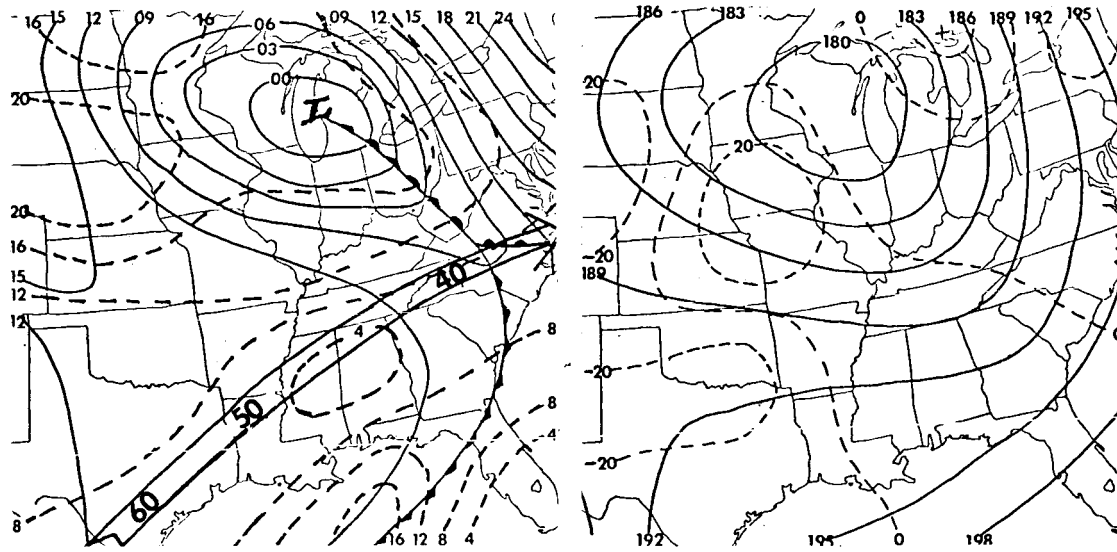

a. Surface chart.

b. 800-mb chart.

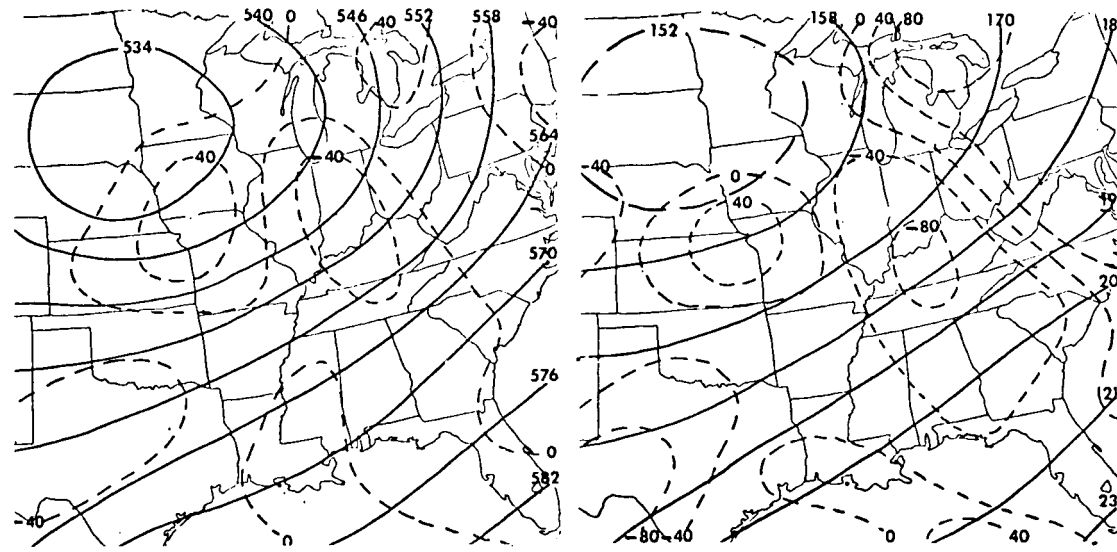

c. 500-mb chart.

d. 200-mb chart.

Fig. 14. Synoptic maps for 0000 GMT, 8 December 1969. (Dashed lines on surface map represent 500-mb vorticity (10^{-5} sec^{-1}). Dashed lines on upper-level maps are values of ω (10^{-4} mb sec^{-1}).)

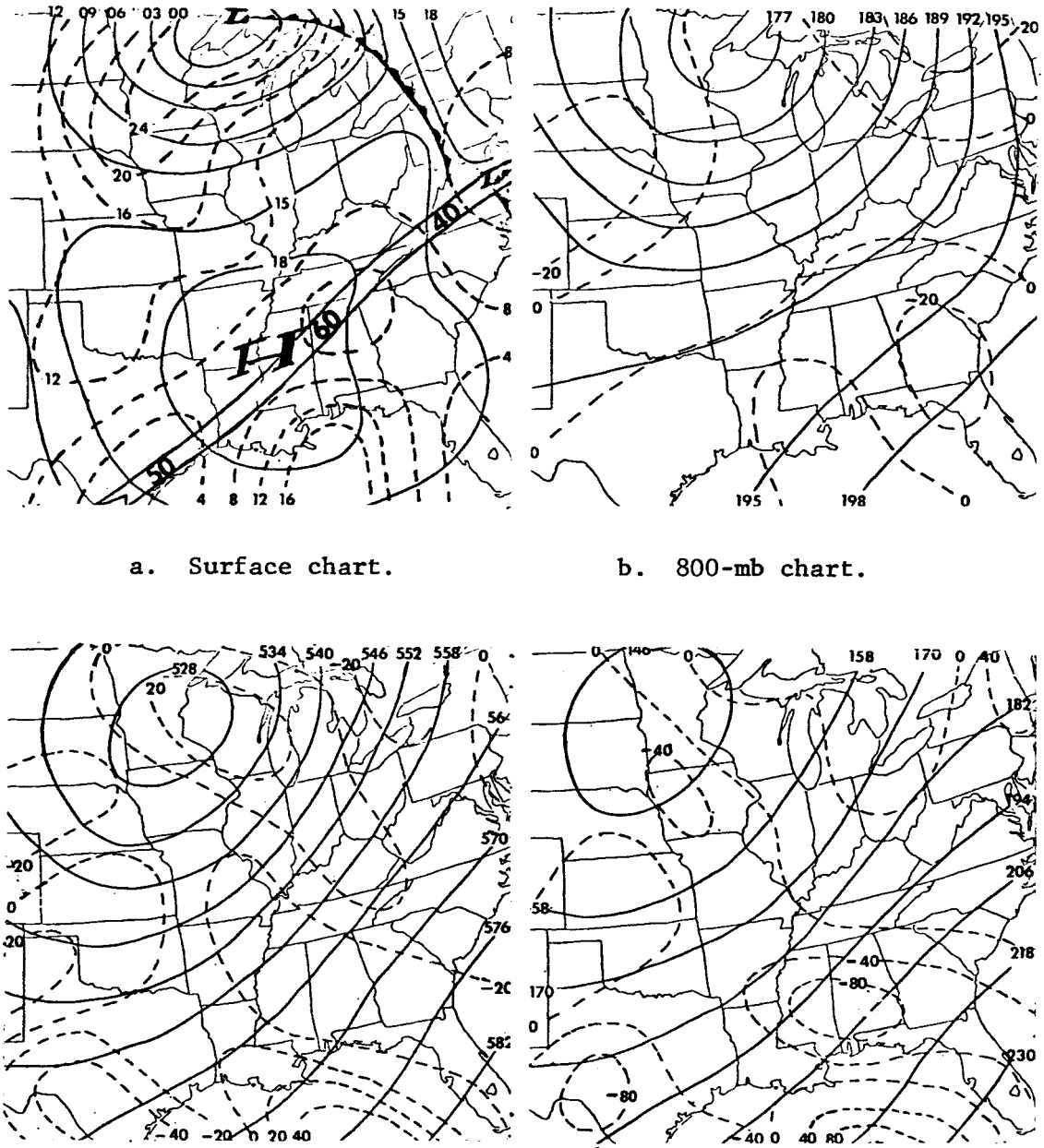

a. Surface chart.

b. 800-mb chart.

c. 500-mb chart.

d. 200-mb chart.

Fig. 15. Synoptic maps for 1200 GMT, 8 December 1969. (Dashed lines on surface map represent 500-mb vorticity (10^{-5} sec^{-1}). Dashed lines on upper-level maps are values of ω (10^{-4} mb sec^{-1}).)

5. DISCUSSION OF RESULTS

a. Kinetic energy budget excluding dissipation

The terms of the kinetic energy budget equation (Eq. 36), except for dissipation, are shown in Figs. 16 to 20 for Case I and in Figs. 21 to 27 for Case II. The solid lines represent the conversion of potential energy into kinetic energy, and the dashed lines represent the horizontal component of the boundary flux term, $H(K_h)$. The stippled regions denote areas where the vertical component of the boundary flux term is greater than 20 watts m^{-2}. The position of the low center and its associated frontal system is shown in the upper left frame in each of these figures. In the discussion that follows, layer 1 will be used to refer to the 1000- to 700-mb layer, layer 2 to the 700- to 400-mb layer, and layer 3 to the 400- to 100-mb layer.

1) Conversion terms - Case I. - At 1200 GMT on 1 November 1966, the significant item to note is the large conversion values in layers 2 or 3 over the southeastern United States (Fig. 16b and 16c). The maximum conversion rates in layer 2 appear just to the west of those in layer 3, atypical of the vertical tilt characteristic of extratropical cyclones in the eastern United States. The conversion term in layer 1 appears to be insignificant at this time.

In Fig. 17, which is for 0000 GMT on 2 November 1966, the large conversion rates still are apparent, but the patterns have

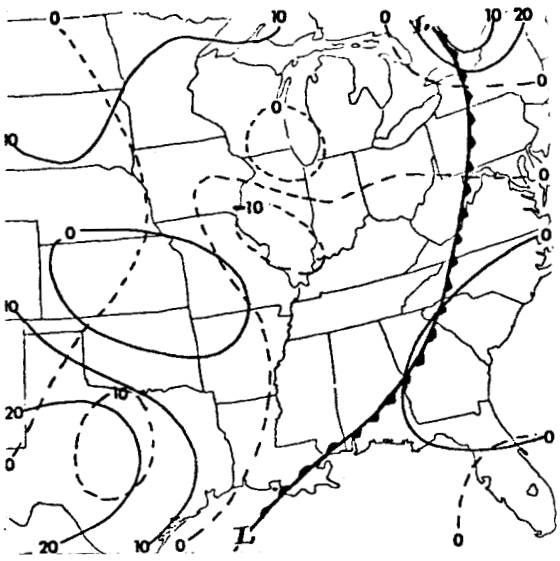

a. 1000-700 mb.

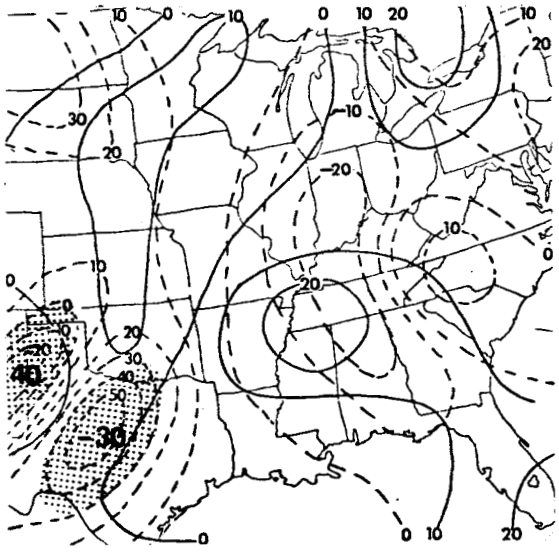

b. 700-400 mb.

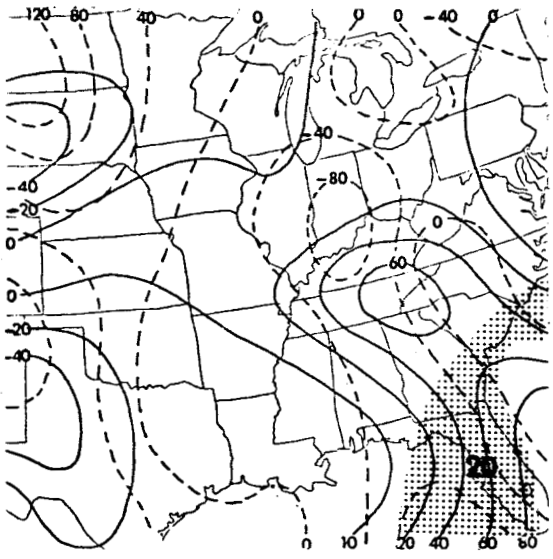

c. 400-100 mb.

Fig. 16. Synoptic maps of kinetic energy budget terms for 1200 GMT, 1 November 1966. (Solid lines represent $C(\pi, K_h)$; dashed lines represent $H(K_h)$; and stippled areas represent regions where $VF(K_h)$ is greater than 20. All values represent integrated values through the given layer expressed in watts m^{-2}.)

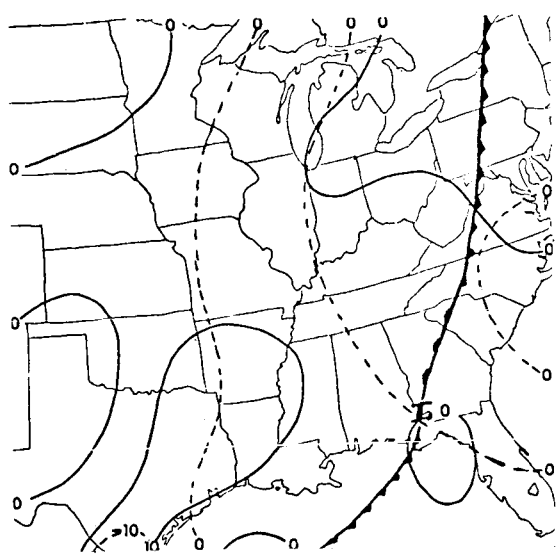

a. 1000-700 mb.

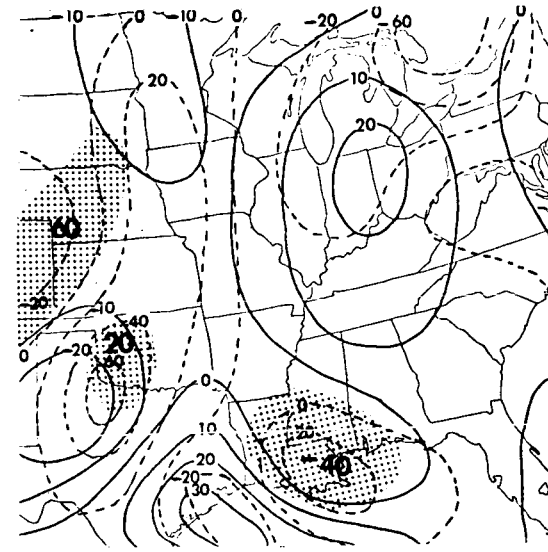

b. 700-400 mb.

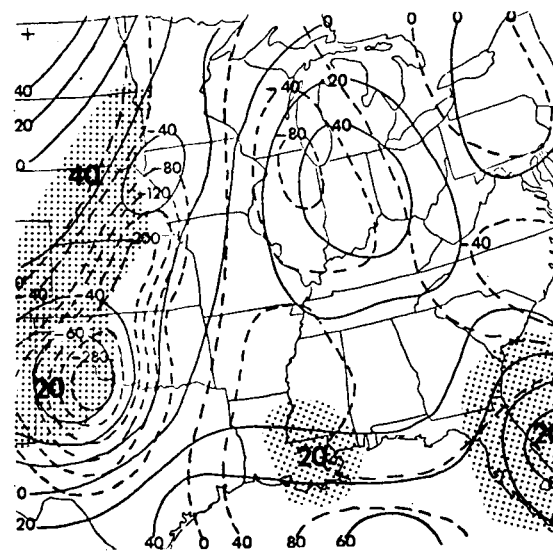

c. 400-100 mb.

Fig. 17. Synoptic maps of kinetic energy budget terms for 0000 GMT, 2 November 1966. (Solid lines represent $C(\pi, K_h)$; dashed lines represent $H(K_h)$; and stippled areas represent regions where $VF(K_h)$ is greater than 20. All values represent integrated values through the given layer expressed in watts m^{-2}.)

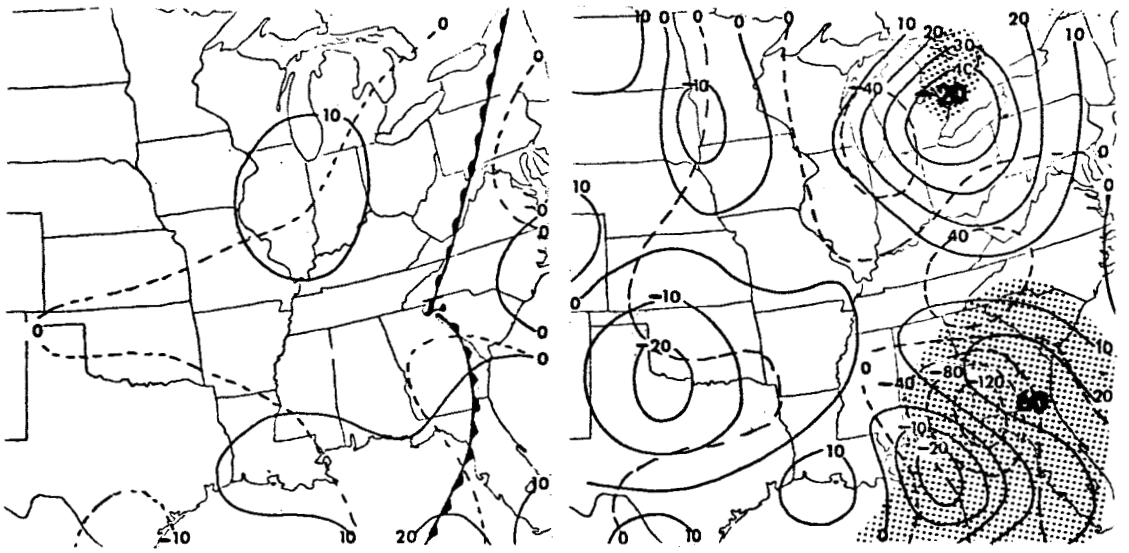

a. 1000-700 mb. b. 700-400 mb.

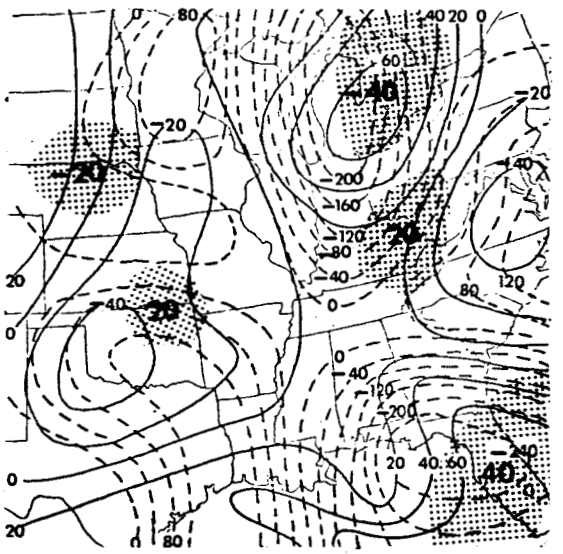

c. 400-100 mb.

Fig. 18. Synoptic maps of kinetic energy budget terms for 1200 GMT, 2 November 1966. (Solid lines represent $C(\pi, K_h)$; dashed lines represent $H(K_h)$; and stippled areas represent regions where $VF(K_h)$ is greater than 20. All values represent integrated values through the given layer expressed in watts m^{-2}.)

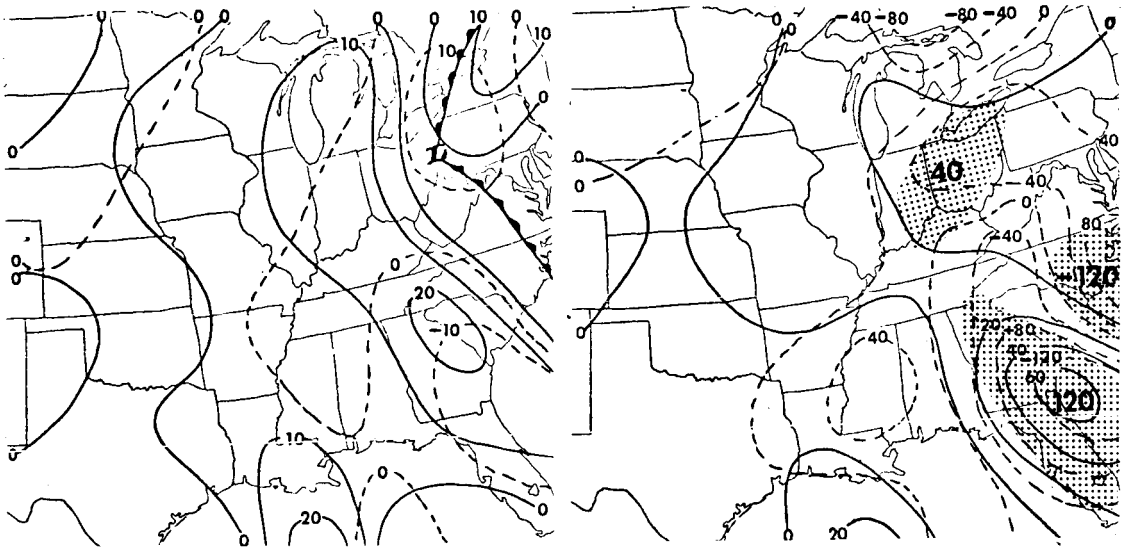

a. 1000-700 mb.

b. 700-400 mb.

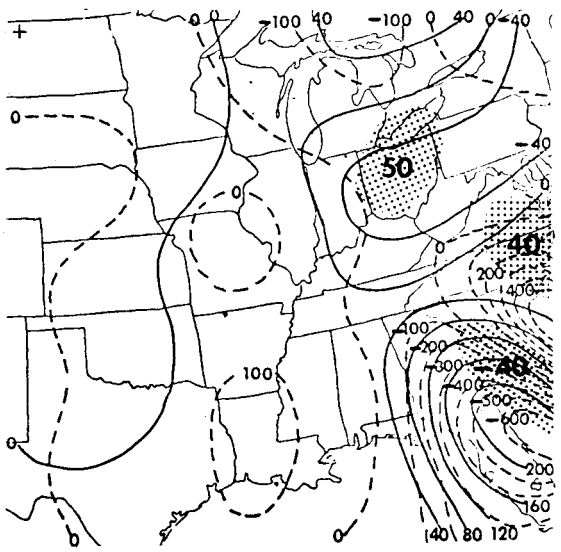

c. 400-100 mb.

Fig. 19. Synoptic maps of kinetic energy budget terms for 0000 GMT, 3 November 1966. (Solid lines represent $C(\pi, K_h)$; dashed lines represent $H(K_h)$; and stippled areas represent regions where $VF(K_h)$ is greater than 20. All values represent integrated values through the given layer expressed in watts m^{-2}.)

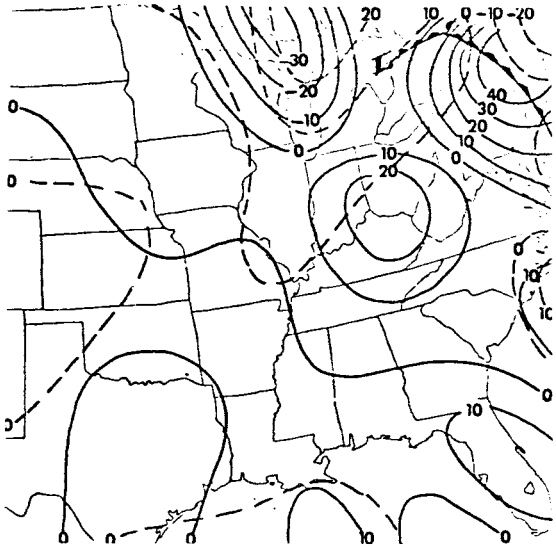

a. 1000-700 mb.

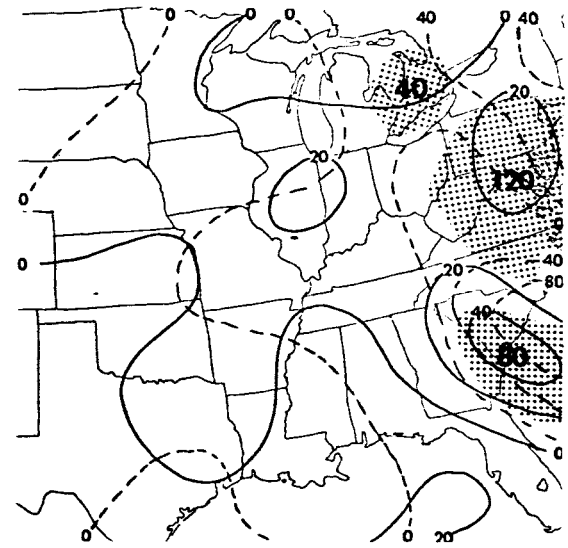

b. 700-400 mb.

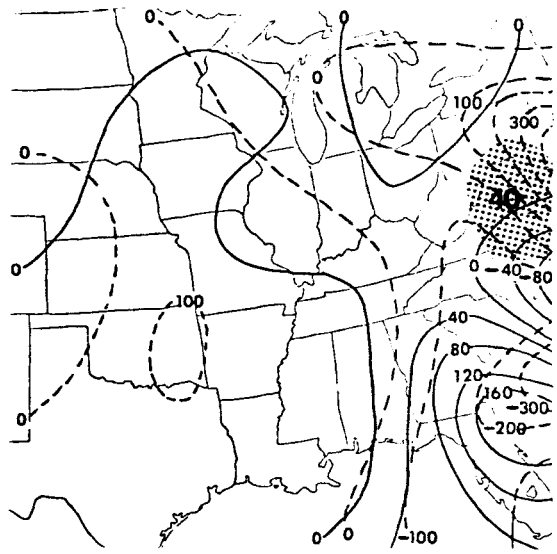

c. 400-100 mb.

Fig. 20. Synoptic maps of kinetic energy budget terms for 1200 GMT, 3 November 1966. (Solid lines represent $C(\pi, K_h)$; dashed lines represent $H(K_h)$; and stippled areas represent regions where $VF(K_h)$ is greater than 20. All values represent integrated values through the given layer expressed in watts m^{-2}.)

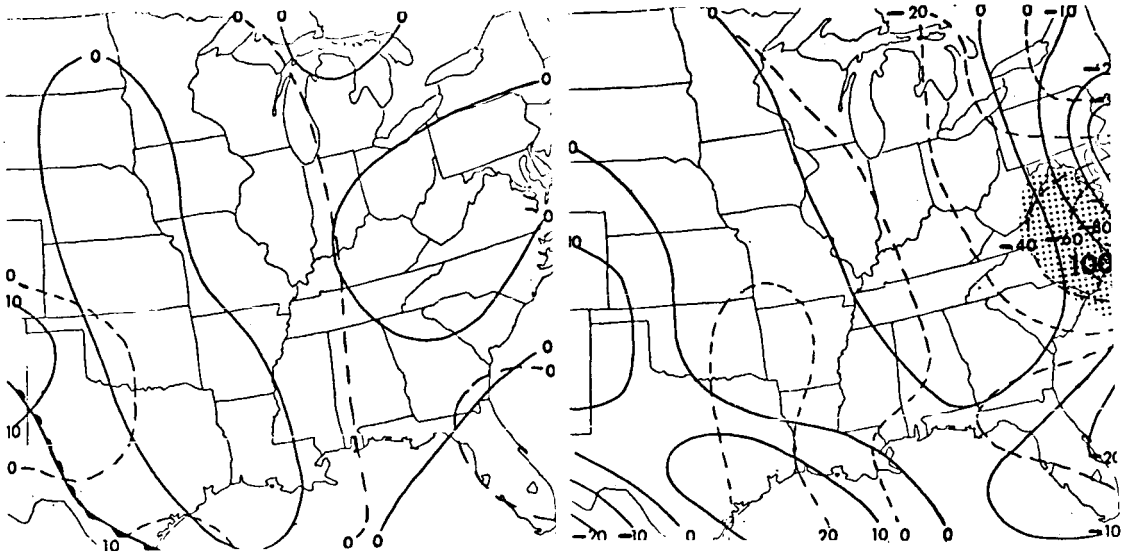

a. 1000-700 mb.

b. 700-400 mb.

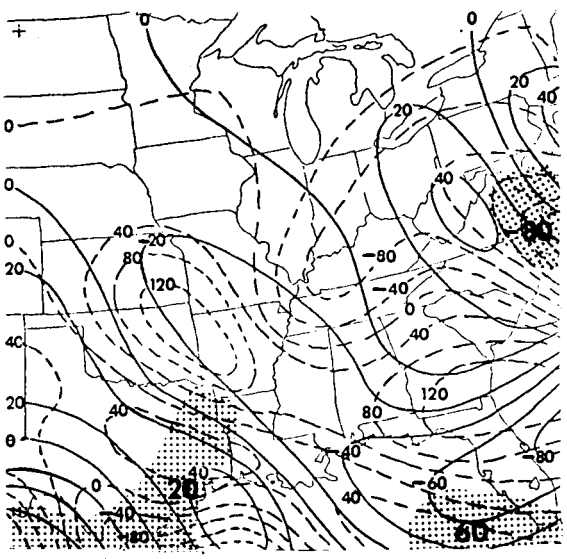

c. 400-100 mb.

Fig. 21. Synoptic maps of kinetic energy budget terms for 1200 GMT, 5 December 1969. (Solid lines represent $C(\pi, K_h)$; dashed lines represent $H(K_h)$; and stippled areas represent regions where $VF(K_h)$ is greater than 20. All values represent integrated values through the given layer expressed in watts m^{-2}.)

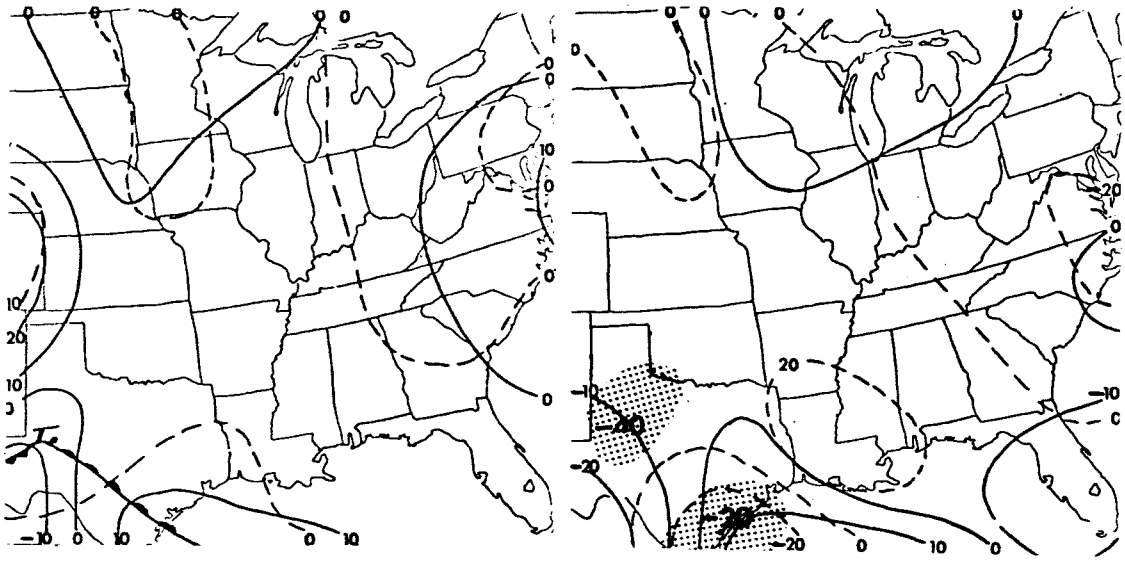

a. 1000-700 mb.

b. 700-400 mb.

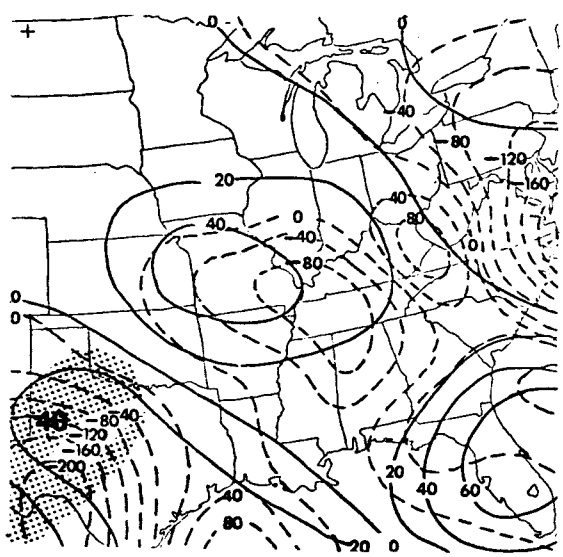

c. 400-100 mb.

Fig. 22. Synoptic maps of kinetic energy budget terms for 0000 GMT, 6 December 1969. (Solid lines represent $C(\pi, K_h)$; dashed lines represent $H(K_h)$; and stippled areas represent regions where $VF(K_h)$ is greater than 20. All values represent integrated values through the given layer expressed in watts m^{-2}.)

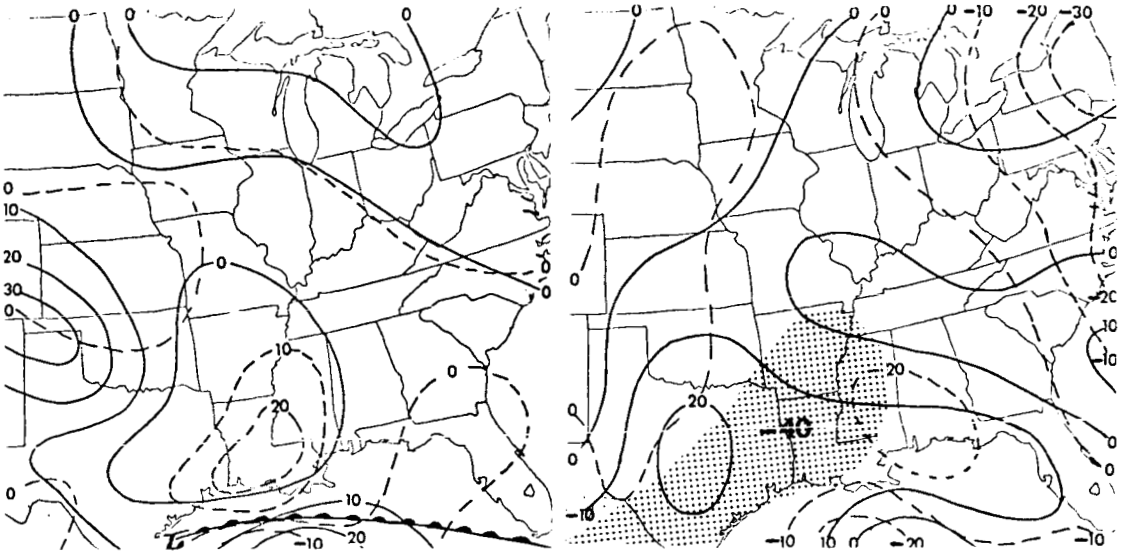

a. 1000-700 mb. b. 700-400 mb.

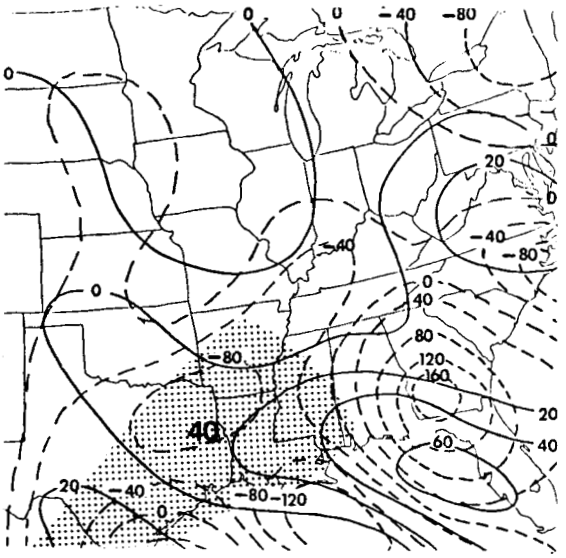

c. 400-100 mb.

Fig. 23. Synoptic maps of kinetic energy budget terms for 1200 GMT, 6 December 1969. (Solid lines represent $C(\pi, K_h)$; dashed lines represent $H(K_h)$; and stippled areas represent regions where $VF(K_h)$ is greater than 20. All values represent integrated values through the given layer expressed in watts m^{-2}.)

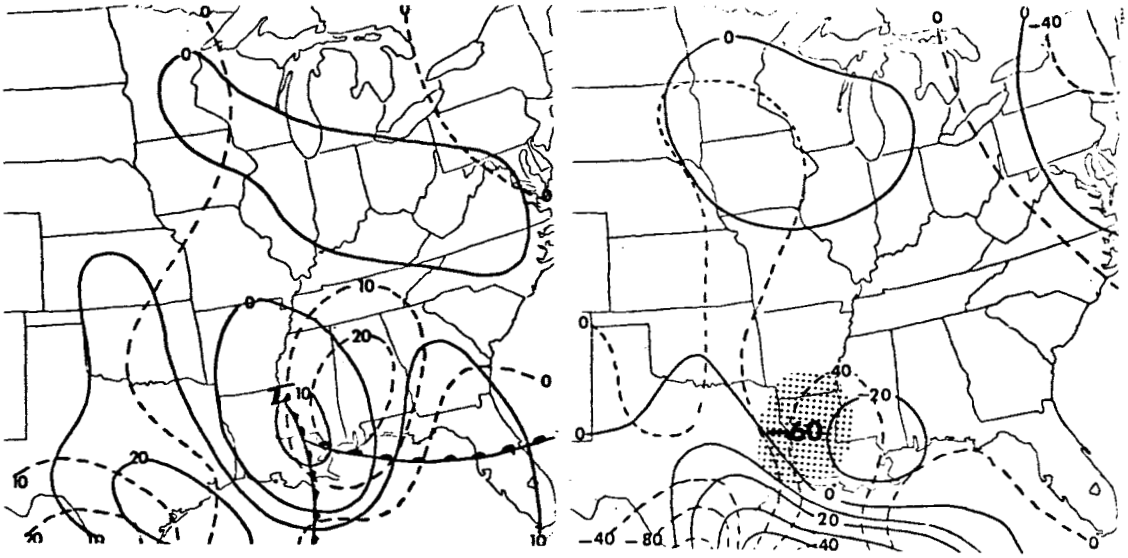

a. 1000-700 mb.

b. 700-400 mb.

c. 400-100 mb.

Fig. 24. Synoptic maps of kinetic energy budget terms for 0000 GMT, 7 December 1969. (Solid lines represent $C(\pi, K_h)$; dashed lines represent $H(K_h)$; and stippled areas represent regions where $VF(K_h)$ is greater than 20. All values represent integrated values through the given layer expressed in watts m^{-2}.)

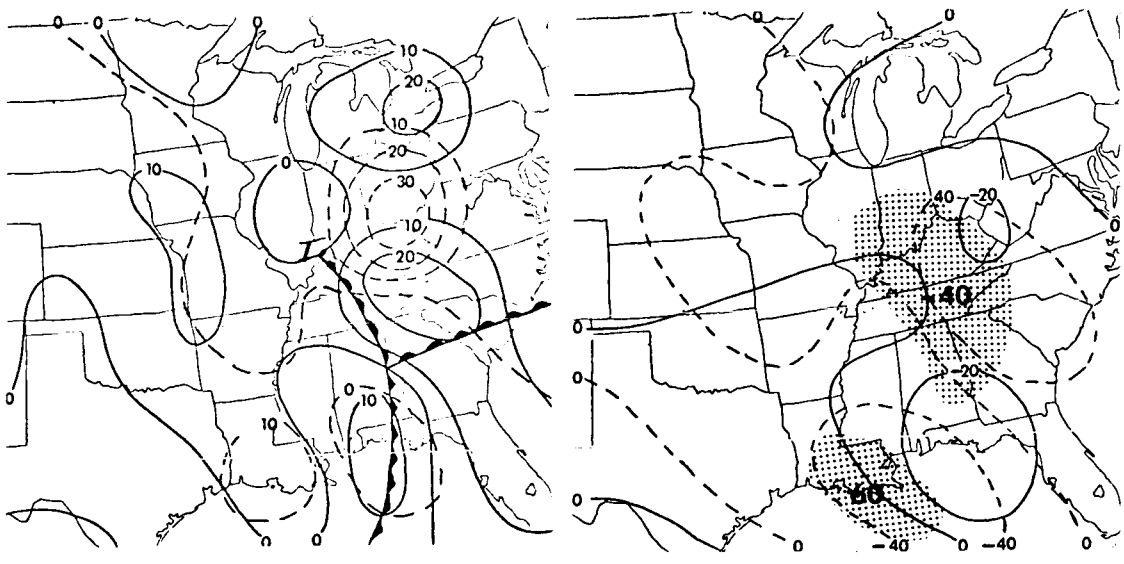

a. 1000-700 mb. b. 700-400 mb.

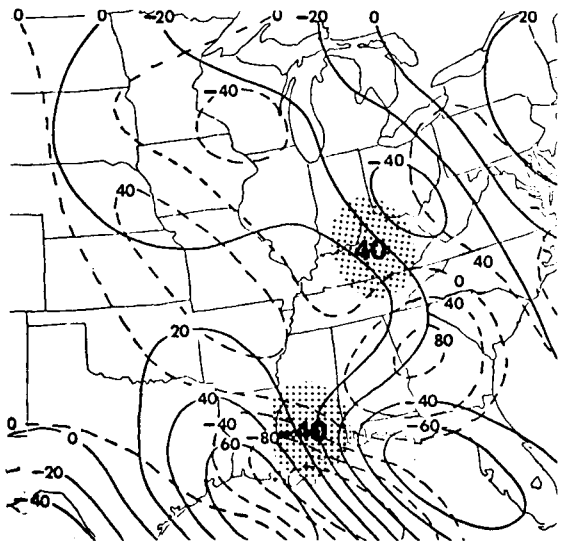

c. 400-100 mb.

Fig. 25. Synoptic maps of kinetic energy budget terms for 1200 GMT, 7 December 1969. (Solid lines represent $C(\overline{\Pi},K_h)$; dashed lines represent $H(K_h)$; and stippled areas represent regions where $VF(K_h)$ is greater than 20. All values represent integrated values through the given layer expressed in watts m^{-2}.)

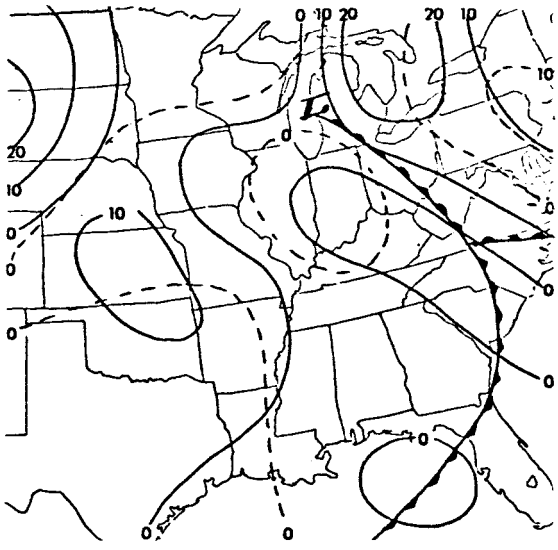

a. 1000-700 mb.

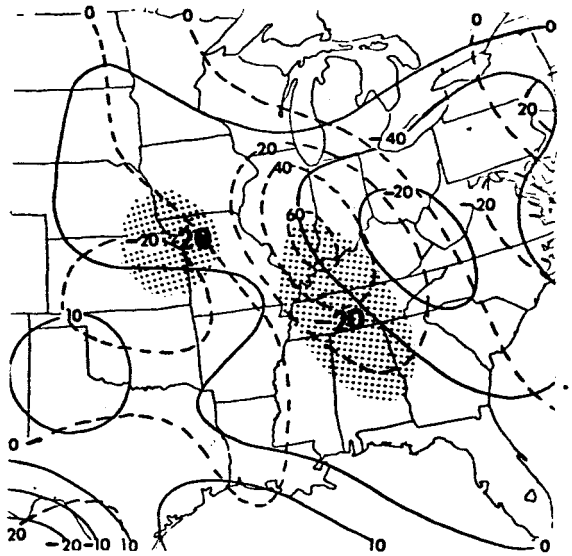

b. 700-400 mb.

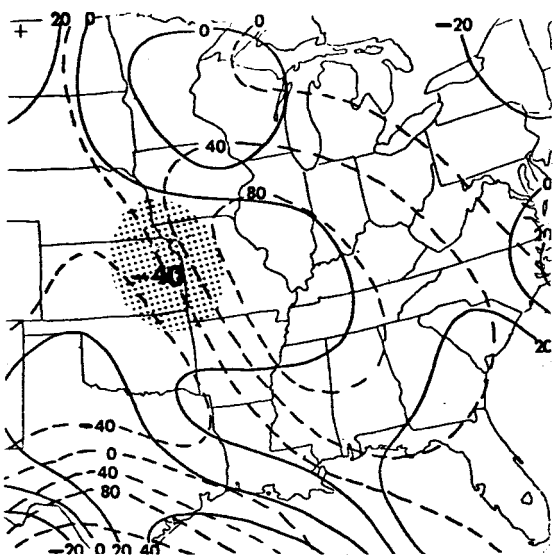

c. 400-100 mb.

Fig. 26. Synoptic maps of kinetic energy budget terms for 0000 GMT, 8 December 1969. (Solid lines represent $C(\pi, K_h)$; dashed lines represent $H(K_h)$; and stippled areas represent regions where $VF(K_h)$ is greater than 20. All values represent integrated values through the given layer expressed in watts m^{-2}.)

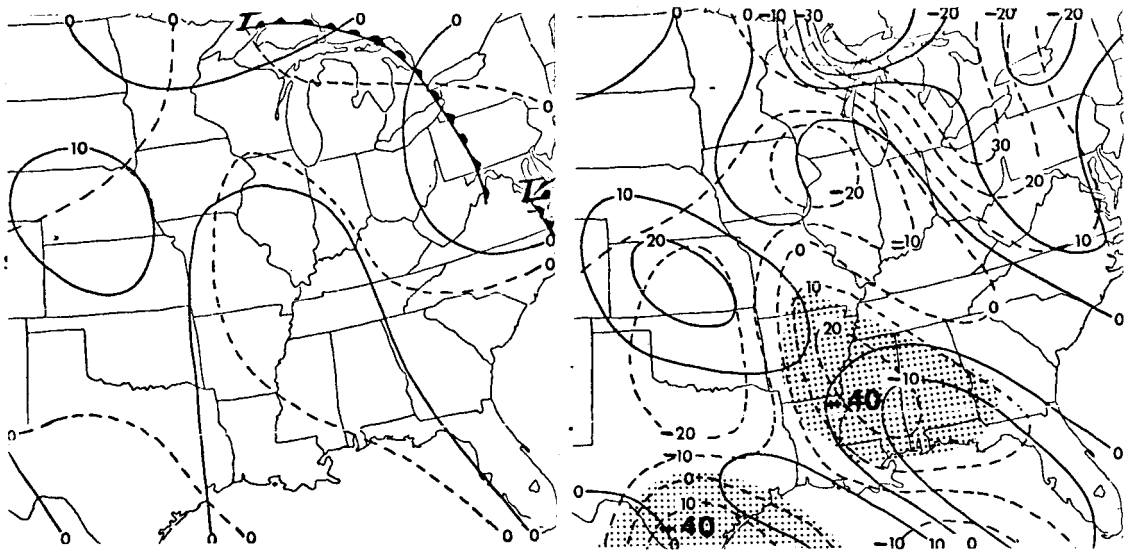

a. 1000-700 mb.

b. 700-400 mb.

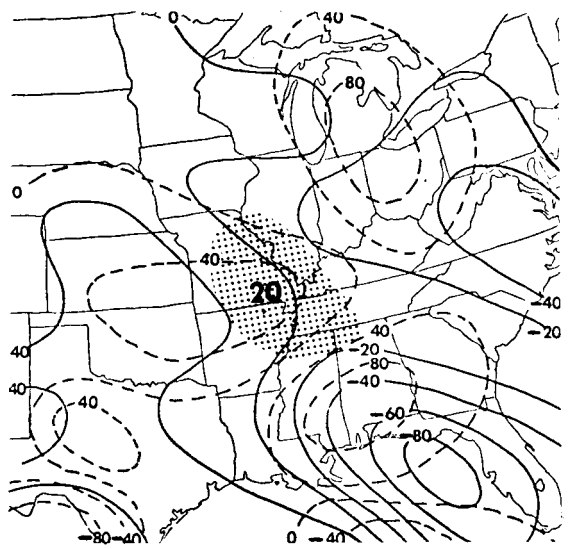

c. 400-100 mb.

Fig. 27. Synoptic maps of kinetic energy budget terms for 1200 GMT, 8 December 1969. (Solid lines represent $C(\pi, K_h)$; dashed lines represent $H(K_h)$; and stippled areas represent regions where $VF(K_h)$ is greater than 20. All values represent integrated values through the given layer expressed in watts m^{-2}.)

changed somewhat. The center of maximum conversion in layer 2 has moved northward into Indiana, and the center in layer 3 has split into two parts, one off the east coast of Florida, and one in Indiana. Conversion rates in layer 1 still are small.

By 1200 GMT on 2 November (Fig. 18, p. 53), the conversion rates have increased in layer 1 to the south of the surface low center. The centers of positive conversion in layers 2 and 3 have moved slowly northward and the maximum values have increased by about 20 watts m^{-2}. The two centers in layer 3 are becoming separated by large negative values.

In Fig. 19, (p. 54), which is for 0000 GMT on 3 November, dramatic changes have occurred in all three layers. Significant conversion of potential energy into kinetic energy is very prominent in layer 1 in the vicinity of the low center. In layers 2 and 3 the large conversion rates no longer appear above the surface low. The only large conversion values now appear over Florida in association with the jet stream.

In the final figure in this series, Fig. 20 (p. 55), the low has reached its maximum intensity and has begun to dissipate slowly. The conversion term has become negative in the vicinity of the low center thus indicating a conversion of kinetic energy into potential energy in layer 1 of the cyclone. In layers 2 and 3 the conversion term is small above the low center.

2) Boundary flux terms - Case I. - At 1200 GMT on 1 November, the horizontal component of the boundary flux term is large and negative in layer 3 over the southeastern United States thereby indicating that most of the kinetic energy that is being generated in this region is being transported out of the region. However, in the extreme southeastern United States, the vertical component of the boundary flux is large and positive which implies that kinetic energy is being concentrated in layer 3. Since the vertical motion is downward in this area (see Fig. 3d, p. 35), there is also a considerable downward flux of kinetic energy in northern Florida and southern Alabama during this time. It is significant to note that this is the area in which cyclogenesis will begin to occur in about 12 hours. The horizontal component of the boundary flux term is large and negative in layer 2 in the east central United States, matching exactly the positive conversion rates present in that area (Fig. 16b, p. 51). The vertical component of the boundary flux term is positive in layer 2 throughout the southeastern United States, but since the values are all less than 20 watts m^{-2}, this area does not appear in Fig. 16b (p. 51). Finally, both components of the boundary flux term appear to be insignificant in layer 1.

By 1200 GMT on 2 November (Fig. 18, p. 53), the horizontal component of the boundary flux term in layer 3 has increased over the southeastern United States to the point where more than

five times as much kinetic energy is being removed horizontally as is being generated. The vertical component of the boundary flux term in layer 2 has increased to more than 60 watts m^{-2} in the southeastern United States. Coupled with the downward vertical motion that is evident in Fig. 5c (p. 38), it is apparent that there is a significant downward flux of kinetic energy through layer 2 in this area. This represents a lag of about 24 hours from the time that the large downward flux was evident in layer 3.

In the final two figures in this series, Figs. 19 and 20 (pp. 54 and 55), a general decrease in the values of the boundary flux term can be noted in layers 2 and 3, except in the vicinity of the jet stream where both the horizontal and vertical components of the boundary flux term remain large. In Fig. 19 (p. 54), the vertical component of the boundary flux term is large in layers 2 and 3 over Ohio. From Fig. 6 (p. 39) it can be seen that the vertical motion is upward in this area, thereby implying that kinetic energy in this region is being transported upward now rather than downward as on 1 and 2 November. These areas still are apparent in Fig. 20 (p. 55), but have shifted to the north and east and have become smaller in size. The horizontal component of the boundary flux term in layer 1 remained relatively insignificant until 1200 GMT on 3 November. At this time it can be seen in Fig. 20 (p. 55) that kinetic energy is being concentrated

by this term in layer 1 on the western side of the low, while the reverse is true on the eastern side of the low.

3) Summary of kinetic energy budget for Case I. - At this point it would be appropriate to reconstruct the steps that occurred during the development of this cyclone. Prior to the initiation of cyclogenesis at the surface, kinetic energy was being generated in the upper levels of the atmosphere over northern Florida. A significant portion of this energy was transported downward through the atmosphere where it supplied kinetic energy to the lower levels. Note the rapid increase in the 500-mb vorticity values in the Gulf of Mexico from 1200 GMT on 1 November 1966 (Fig. 3a, p.35) to 0000 GMT on 2 November 1966 (Fig. 4a, p. 36) which indicates the strengthening of the 500-mb circulation just prior to cyclogenesis at the surface. As the cyclone began to develop, vertical velocities were generated that provided the direct circulation necessary for the conversion of potential energy into kinetic energy in the low levels of the cyclone. As the cyclone reached the mature stage, the upward vertical motions extended into the cold air and resulted in a conversion of kinetic energy into potential energy. The modification of the cyclone by frictional dissipation and diabatic processes will be discussed later.

4) Conversion term - Case II. - The kinetic energy budget for the second synoptic case is shown starting with Fig. 21 (p. 56) which presents conditions for 1200 GMT on 5 December 1969. The first

item to note in Fig. 21 (p. 56) is the presence of areas of significant conversion of potential energy to kinetic energy in all three layers to the north of the warm front through southwestern Texas. These positive values of conversion are nearly balanced in layers 2 and 3 by the negative values which appear to the south of the front.

By 0000 GMT on 6 December (Fig. 22, p. 57), the conversion pattern in layer 1 has changed so that there is now positive conversion on both sides of the warm front and to the north of the low center. The conversion values in layer 3 have become much smaller over Texas, while those in layer 2 have remained unchanged.

During the next 24 hours a significant change occurred in the conversion term. This change can be seen in Figs. 23 and 24 (pp. 58 and 59) which depict conditions for 1200 GMT on 6 December and 0000 GMT on 7 December. The important change that occurred was the appearance of negative conversion values in layers 1 and 2 in the vicinity of the cyclone center. Apparently an indirect circulation (cold air rising) existed in this region of the cyclone that resulted in a conversion of kinetic energy into potential energy. The area of upward vertical motion to the northeast of the cyclone center (Fig. 11, p. 45) seems to substantiate this idea.

By 1200 GMT on 7 December (Fig. 25, p. 60), the low center has moved into southern Illinois and areas of positive conversion

appear on all sides of the cyclone in layer 1. In layers 2 and 3, however, small negative conversion rates are present above the cyclone center.

5) Boundary flux term - Case II. - In Fig. 21 (p. 56), the horizontal component of the boundary flux term is large and positive in layers 1, 2, and 3 over southeastern Texas and the Gulf of Mexico, thereby indicating an increase in the concentration of kinetic energy at all levels in this region. The vertical component of the boundary flux term also is positive over this region, and by referring to Fig. 9d (p. 43), one can see that the vertical motion is upward in this area from which it can be inferred that kinetic energy is being transported upward in the high levels of the cyclone.

The most noticeable change during the next 12 hours is the appearance of large negative values of the horizontal component of the boundary flux term in western Texas (Fig. 22, p. 57). The vertical component of the boundary flux term still is large and positive in layer 3 over Texas, but the center has shifted northward. In layer 2, two areas can be seen where the vertical component of the boundary flux term is large and negative. Since the vertical motion generally is upward in this area (Fig. 10c, p. 44), it appears that kinetic energy now is being transported upward through both layers 2 and 3.

In Figs. 23 and 24 (pp. 58 and 59), the vertical component of the boundary flux term is much more apparent over the middle and high levels of the cyclone. An extensive area of upward vertical motion at 800 and 500 mb to the east of the cyclone center can be seen in Figs. 11 and 12 (pp. 45 and 46). Upward vertical motion also exists at 100 mb, but the magnitude is smaller. This pattern of vertical motion results in an upward flux of kinetic energy that produces the increase in intensity of the jet stream, as shown in Figs. 11a and 12a (pp. 45 and 46). In both Figs. 23 and 24 (pp. 58 and 59), the horizontal component of the boundary flux term is large and positive in layer 1 to the northeast of the cyclone center thus indicating an increase in the concentration of kinetic energy in this region.

By 1200 GMT on 7 December (Fig. 25, p. 60), the boundary flux terms indicate horizontal convergence of kinetic energy in layers 1 and 2 on the eastern side of the low center. There still is a significant vertical transport of kinetic energy from low to high levels of the cyclone, but the area of vertical transport had decreased.

In Figs. 26 and 27 (pp. 61 and 62), a general decrease in both components of the boundary flux terms can be noted in all layers of the cyclone. The only significant values appear to the south of the cyclone center in association with the jet stream.

6) Summary of kinetic energy budget for Case II. - Significant low- and middle-level conversion rates were apparent throughout the development of the cyclone in Case II. Boundary fluxes then were instrumental in producing an increasing concentration of kinetic energy in the eastern positions of the cyclone, particularly in the low and middle levels. Part of this kinetic energy was transported upward into the jet stream level and then transported horizontally out of the region. As will be seen later, part of this kinetic energy also was dissipated by frictional forces. As the conversion rates decreased late in the life of the cyclone, the gradients of kinetic energy decreased throughout the cyclone and resulted in a decrease in both components of the boundary flux terms.

7) Comparison of kinetic energy budget in Cases I and II. - Case I was characterized by large positive conversion rates in the upper levels of the cyclone during the initial development stage. A significant portion of the kinetic energy generated at the high levels was transported downward through the atmosphere, thus supplying a source of energy for the lower levels. As the development of the cyclone continued, the upper-level conversion rates decreased whereas positive low-level conversion rates became more apparent.

The upper-level conversion rates were much smaller in the second synoptic case whereas positive conversion in the low levels

of the cyclone could be noted throughout the development stage. In contrast to Case I, kinetic energy in Case II was transported upward through the atmosphere during the early stages of development; this resulted in an increase in intensity of the jet stream. A further comparison between the two cases is presented in Fig. 28. The plot of kinetic energy versus time is shown for the two synoptic cases in this figure. The solid lines represent the average kinetic energy within a 500-km radius of the cyclone center, while the dashed lines represent average kinetic energy within a 1000-km radius.

There are two features of the kinetic energy traces shown in Fig. 28a that should be noted. First, the solid lines show that the maximum kinetic energy in layer 3 occurred about 12 hours before the maximum value was reached in layer 2. Similarly, the maximum kinetic energy in layer 2 occurred about 24 hours before the maximum value was reached in layer 1. The second significant feature is the differences between the solid and dashed lines for layers 2 and 3. In both of these layers, the maximum value in the dashed lines occurs about 18 hours after the one in the solid lines. The maximum values shown by the dashed lines also are larger than the corresponding ones shown by the solid lines.

The above observations give additional support to the interpretation of the kinetic energy conditions in Case I that was

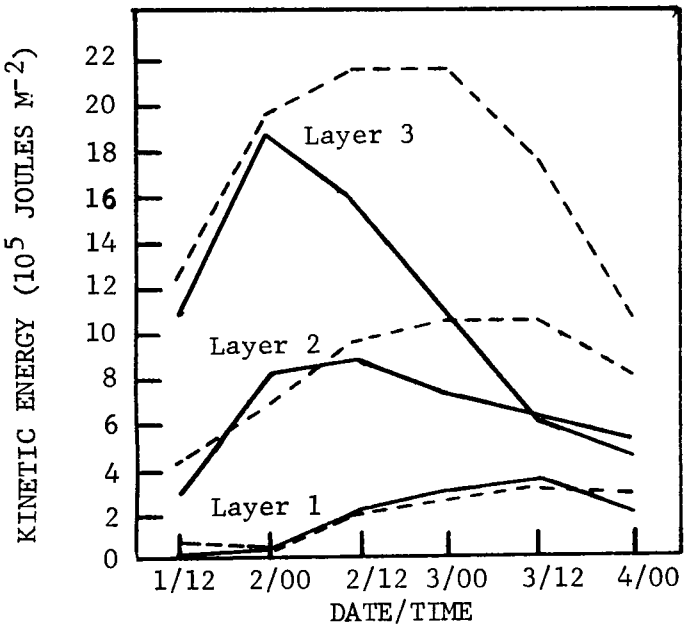

a. November 1966.

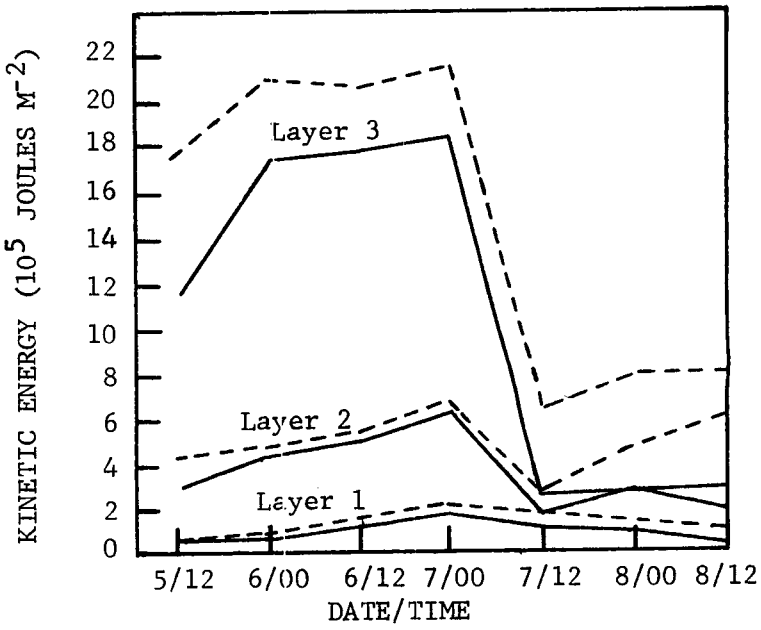

b. December 1969.

Fig. 28. Plot of kinetic energy for the two synoptic cases. (Solid lines represent average kinetic energy within a 500-km radius of the cyclone center; dashed lines represent averages within a 1000-km radius.)

given previously. The conclusion that kinetic energy was generated first in the high levels of the atmosphere and then transported downward may be inferred from the graphs in Fig. 28a (p. 72). The transport of kinetic energy from high to low levels of the atmosphere would account for the observed lag in the peaks of the kinetic energy traces shown in Fig. 28a (p. 72). The importance of the boundary flux terms in layers 2 and 3 also are demonstrated by this figure. That kinetic energy was transported outward from the center of the storm is suggested by the observed difference between the solid and dashed lines of Fig. 28a (p. 72).

The corresponding kinetic energy traces for the second synoptic case exhibit much different characteristics. First, the differences between the solid and dashed lines are much less noticeable. Secondly, the peak in all three levels occurred at about the same time, 0000 GMT on 7 November 1966. The fact that the peaks in the three layers occurred simultaneously seems to preclude vertical transport of kinetic energy as being a dominant factor as in Case I. However, as has been pointed out, there was an upward transport of kinetic energy early in the period that contributed to the intensification of the jet stream. This increase in kinetic energy in layer 3 can be noted in Fig. 28b (p. 72) from 0000 GMT on 6 December to 0000 GMT on 7 December. The similarity in the solid and dashed lines in Fig. 28b (p. 72) indicates that the boundary

flux of kinetic energy was of lesser importance in Case II than in Case I.

b. Modifying influences exerted by low-level frictional dissipation and diabatic processes

Synoptic maps of the diabatic heating term and the boundary layer dissipation term for the 1000- to 700-mb layer are presented in Fig. 29 for Case I, and in Fig. 30 for Case II. The solid lines represent values of diabatic heating computed from the thermodynamic equation in the form,

$$\frac{dH}{dt} = c_p \frac{\partial T}{\partial t} + c_p V_2 \cdot \nabla_p T + \left(c_p \frac{\partial T}{\partial p} - \alpha \right) \omega . \qquad (38)$$

The dashed lines represent values of boundary layer dissipation, as computed from (37). The location of the surface low and its associated frontal system also is shown to illustrate the correspondence between low-level diabatic heating and cyclone development.

1) Case I.- At 1200 GMT on 1 November an extensive area of positive generation of potential energy can be noted in eastern Texas (Fig. 29a). This area of positive generation coincides with the precipitation in this area that resulted from the warm moist air of the Gulf of Mexico rising over the frontal system. The fact that the precipitation in eastern Texas corresponds to the upward vertical motion shown in Figs. 3b and 3c (p. 35), attests to the validity of the vertical motion

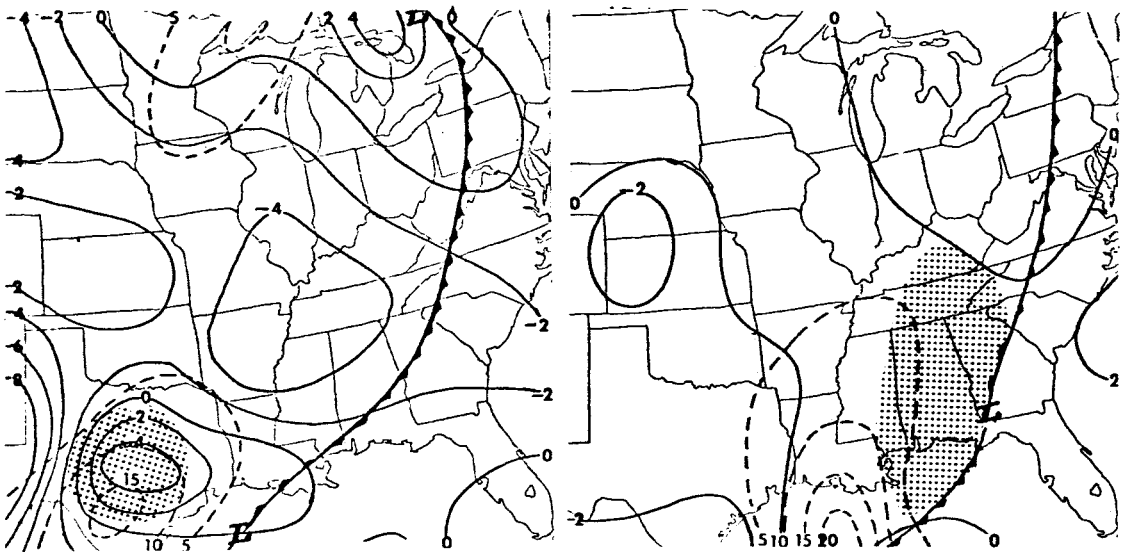

a. 1200 GMT, 1 November 1966 b. 0000 GMT, 2 November 1966

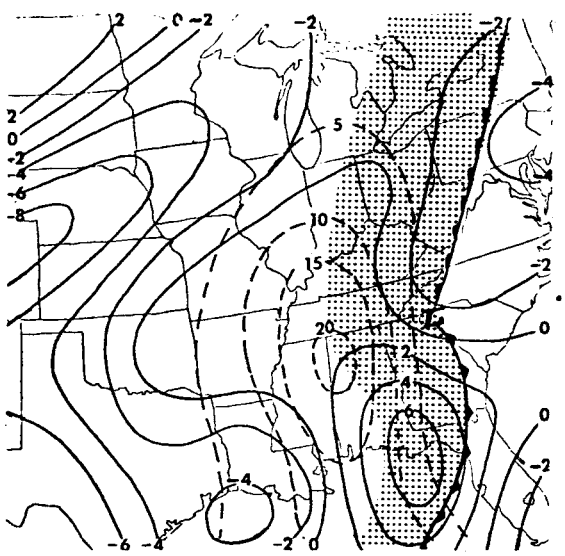

c. 1200 GMT, 2 November 1966

Fig. 29. Synoptic maps of low-level frictional dissipation and diabatic heating for Case I. (Solid lines represent diabatic heating in units of 10^2 watts m^{-2}. Dashed lines are values of frictional dissipation in units of watts m^{-2}. Stippled areas denote precipitation.)

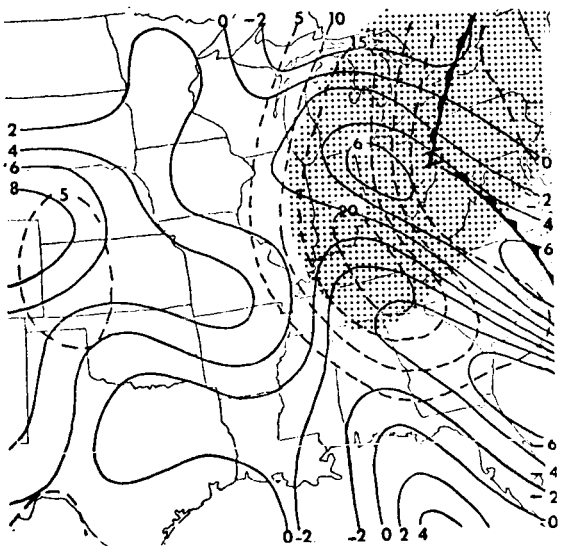

d. 0000 GMT, 3 November 1966

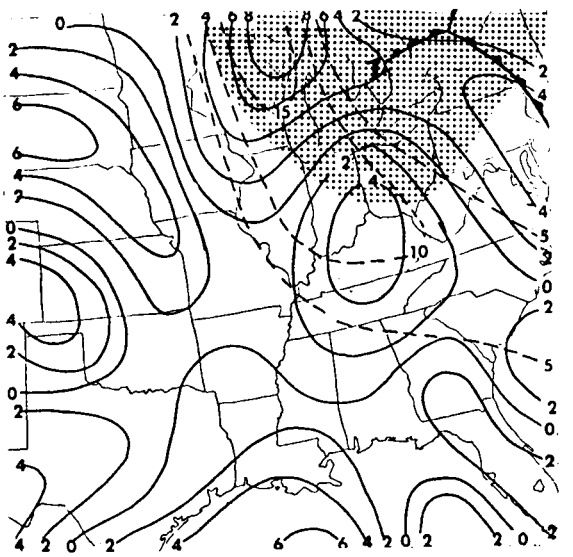

e. 1200 GMT, 3 November 1966

Fig. 29. (continued)

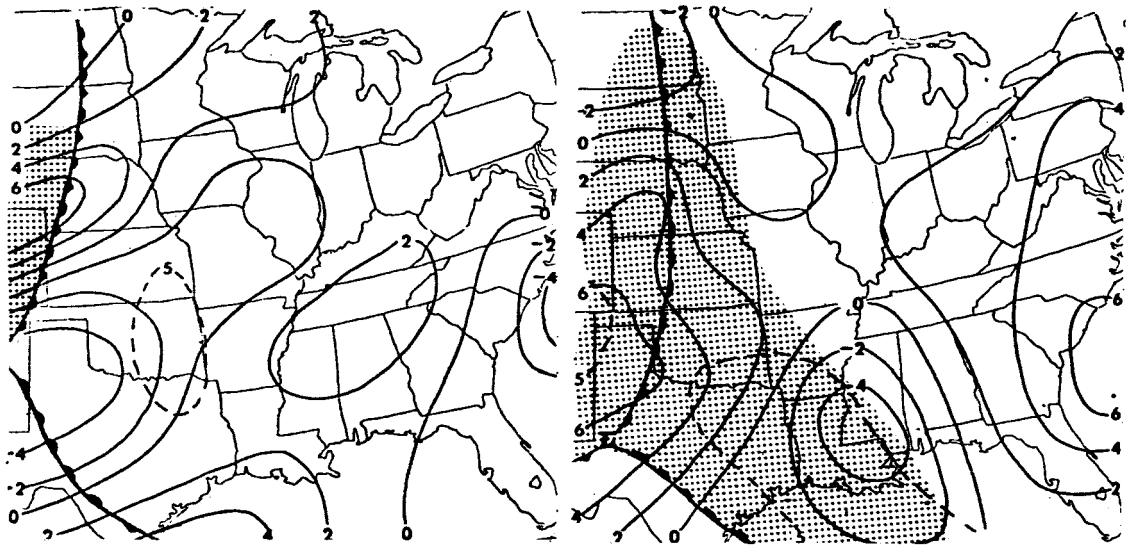

a. 1200 GMT, 5 December 1969 b. 0000 GMT, 6 December 1969

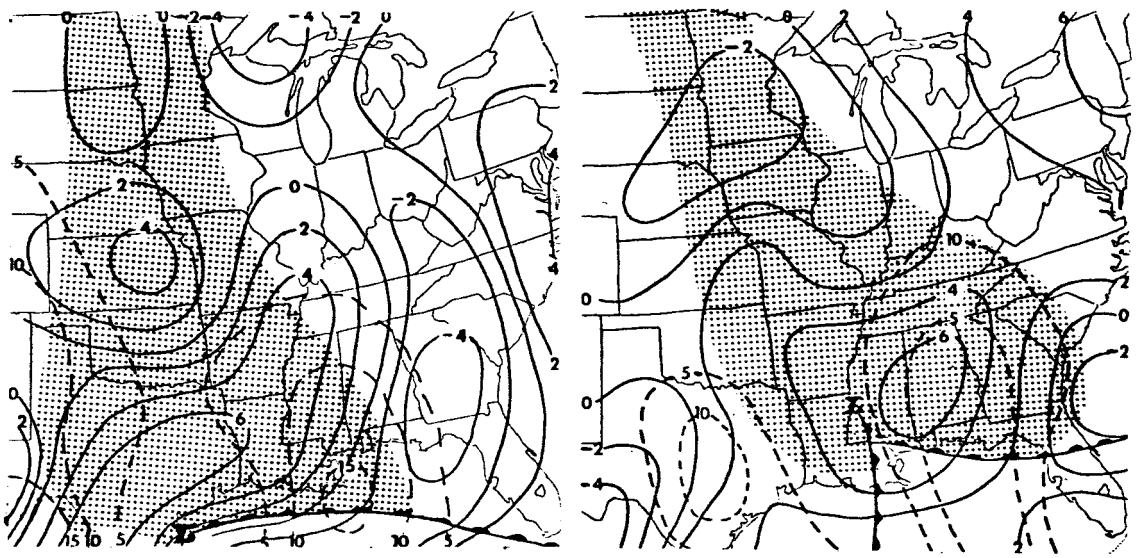

c. 1200 GMT, 6 December 1969 d. 0000 GMT, 7 December 1969

Fig. 30. Synoptic maps of low-level frictional dissipation and diabatic heating for Case II. (Solid lines represent diabatic heating in units of 10^2 watts m^{-2}. Dashed lines are values of frictional dissipation in units of watts m^{-2}. Strippled areas denote precipitation.)

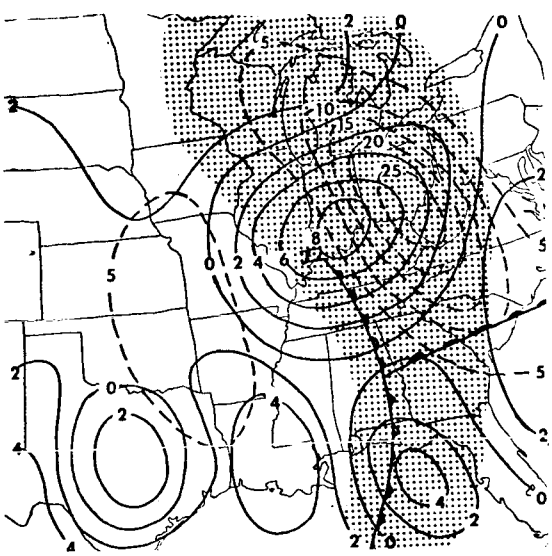

e. 1200 GMT, 7 December 1969

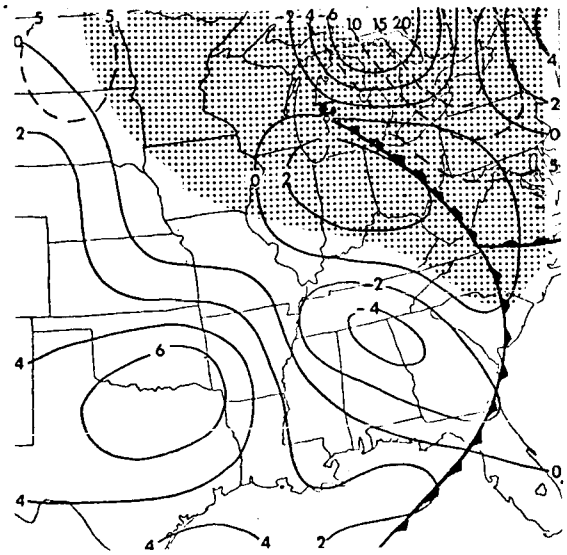

f. 0000 GMT, 8 December 1969

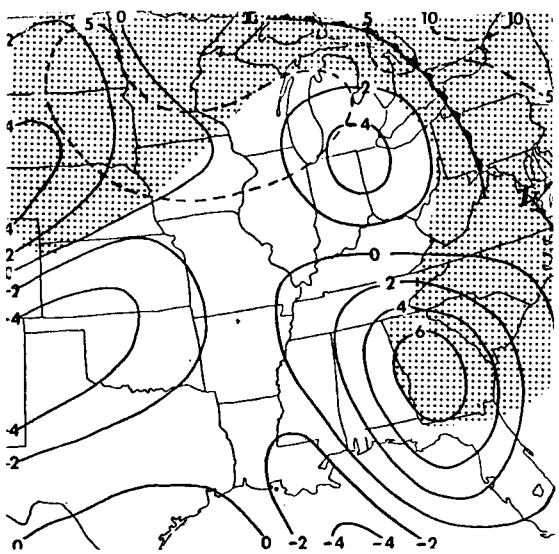

g. 1200 GMT, 8 December 1969

Fig. 30. (continued)

calculations in this region. The large values of boundary layer dissipation in eastern Texas also should be noted. These large values were produced by the increased pressure gradient which resulted in increased wind velocity as the high-pressure ridge moved southward into Texas.

In Fig. 29b (p. 75), the surface low has moved into northern Florida and the diabatic heating term is small over the entire map. There is, however, considerable dissipation in the Gulf of Mexico associated with the strong pressure gradient behind the cold front.

By 1200 GMT on 2 November, the diabatic heating term has become prominent again, exceeding 600 watts m^{-2} in northern Florida (Fig. 29c, p. 75). During this period the low was undergoing rapid development, and the precipitation associated with the low had begun to increase. The boundary layer dissipation had increased also to more than 20 watts m^{-2} in northern Mississippi and Alabama.

The fact that the area of positive generation is south of the low, rather than coincident with the low as would be expected, should be noted. The shift in the center of the area of positive generation away from the low center can be attributed to the manner in which the diabatic heating term was computed. The first term on the right-hand side of (38) was evaluated by subtracting temperatures which were 12 hours apart, whereas the remaining terms

in (37) were evaluated from data at a single time period. Since there was rapid movement of the low center and the cold front during this period, it is likely that large errors in $\frac{\partial T}{\partial t}$ result when using 12-hour backward differences. The values shown in Fig. 29c (p. 75) probably are more representative of average conditions during the 12-hour period 0000 to 1200 GMT on 2 November rather than at 1200 GMT on 2 November. If hourly temperature data were available, it would seem reasonable to expect the areas of diabatic heating to coincide more closely with the low center and its related precipitation pattern. Indeed, in Figs. 29d and 29e (p. 76) this correspondence does exist as the movement of the low center begins to slow down.

In Figs. 29d and 29e (p. 76) the areas of positive generation appear just to the west and north of the low center, closely approximating the precipitation patterns that were present at these times. By 0000 GMT on 3 November, the entire western half of the cyclone is under the influence of large frictional dissipation (Fig. 29d, p. 76). This is approximately the time when the cyclone had reached its maximum intensity. During the next 12 hours the storm decreased in intensity and, as can be noted in Fig. 29e (p. 76), the area of boundary layer dissipation has decreased considerably. At the same time the generation of potential energy by diabatic heating now exceeds 800 watts m^{-2}.

In summary, kinetic energy was being destroyed by low-level frictional dissipation throughout the duration of the cyclone. The maximum dissipation occurred toward the rear of the storm and at about the time when the storm had reached its greatest intensity. As the cyclone reached the mature stage, a significant amount of potential energy was being generated by diabatic processes to the west and north of the cyclone center. The maximum generation occurred to the north of the cyclone center shortly after the cyclone had reached its greatest intensity. The extent to which the potential energy that was generated by diabatic heating was converted into kinetic energy cannot be ascertained precisely since only a small fraction of the potential energy that exists in the atmosphere at any particular time is ever converted into kinetic energy. However, the results that have been presented for Case I do indicate that sufficient potential energy was generated to offset at least a major portion of the frictional dissipation of the cyclone. These results also demonstrate how diabatic processes can serve to prolong the lifetime of an extratropical cyclone.

2) Case II.- In contrast with Case I, the diabatic heating played a significant role throughout the development of the cyclone in Case II. The maximum contribution from diabatic processes appeared at 1200 GMT on 7 December (Fig. 30e, p. 78). This is about 12 hours after the cyclone reached its maximum intensity in terms of kinetic energy (see Fig. 28b, p. 72). After 1200 GMT

on 7 December, the diabatic heating term decreased and became insignificant by the end of the period (1200 GMT on 8 December (Fig. 30g, p. 78)).

The frictional dissipation term was small except for the period 1200 GMT, 7 December to 0000 GMT, 8 December during which time it exceeded 25 watts m^{-2}. The areas of frictional dissipation consistently appear to the east of the low center in sharp contrast to the first case in which the frictional dissipation was concentrated on the western side of the low center.

The differences in the two cases point out the different ways that diabatic processes can affect cyclogenesis. In the first case the diabatic heating term became significant late in the development of the cyclone, and reached its maximum value after the cyclone had become fully developed. It appears that in this case diabatic heating served to prolong the life of the cyclone rather than contributing significantly to the cyclogenesis process. In the second case, however, significant diabatic heating was evident early in the development stage, and apparently was a contributing factor to the initial growth of the cyclone as well as serving to extend the life of the cyclone.

c. Diabatic heating in the middle and high levels of the cyclone

At this point only the diabatic heating for the 1000- to 700-mb layer of the cyclone has been discussed. In Fig. 31, a comparison between the low- and middle-level diabatic heating

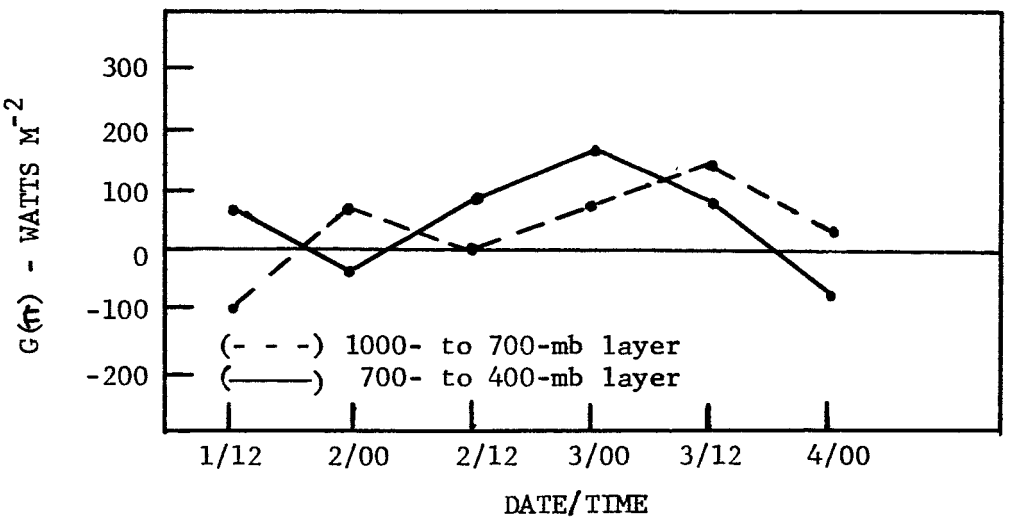

a. November 1966.

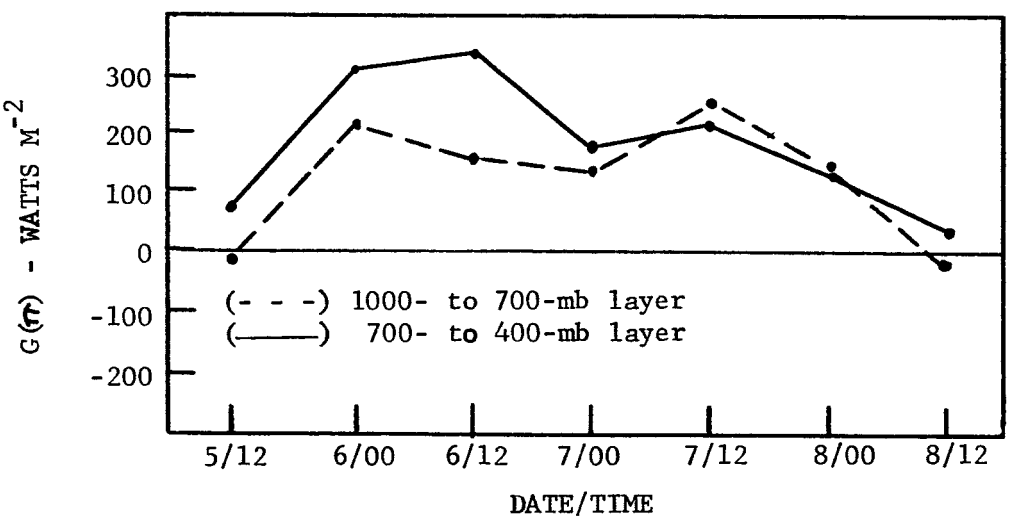

b. December 1969.

Fig. 31. Diabatic heating term. (Values were obtained by averaging diabatic heating term within a 1000-km radius of the cyclone center.)

can be seen. The low-level values are given by the dashed lines and the middle-level values by the solid lines. These values represent averages within a 1000-km radius of the cyclone center. In each of the synoptic cases, the low- and middle-level diabatic heating terms appear to be very similar. The most noticeable difference is that, in both synoptic cases, the diabatic heating is greater in the middle levels of the cyclone during the initial development. The graphs in Fig. 31 (p. 83) again point out the different character of the diabatic heating in the two synoptic cases.

The diabatic heating term for the 400- to 100-mb layer of the cyclone was very erratic in both synoptic cases. The validity of the computations in this layer is highly questionable because of observational errors in the high levels of the atmosphere, particularly at the 100-mb level. The tendency of the kinematic method to overestimate vertical velocities at the 100-mb level has been pointed out by O'Neill (1966) and O'Brien (1970). Also, the temperature and wind data are much less reliable at this level than in the lower levels of the atmosphere. The combination of these factors can produce large errors in the diabatic heating term for the 400- to 100-mb layer of the cyclone. For this reason it was felt that the erratic results for this layer are not representative of actual atmospheric conditions, and consequently they are not presented here in the form that they were for the

other two layers. However, the diabatic heating values for the 400- to 100-mb layer were averaged over the life of the cyclone and within a 1000-km radius of the center. This procedure yielded values of -78 and 190 watts m^{-2} for Cases I and II, respectively. This averaging process removes some of the spurious fluctuations from the data and the average values should be more representative of atmospheric conditions. However, there is no apparent reason why a negative value was obtained in Case I and a positive value in Case II. This difference may be simply a reflection of the errors in the observations.

As a final note, diabatic heating results from release of latent heat during precipitation, short and long wave radiation, and transfer of sensible heat as the cyclone moves over heat sources or sinks. No attempt has been made to separate these components in this study. Qualitatively at least, it could be seen that release of latent heat provided the major contribution to diabatic heating in both synoptic cases because, invariably, large values of diabatic heating were associated with areas of precipitation. Estimates by Anthes and Johnson (1968) indicate that in the case of hurricane Hilda (1954), 77% of the generation of available potential energy resulted from latent heat release, 17% by infrared cooling, and 6% by direct solar absorption. Sensible heat exchange at the surface of Earth was found to be a negligible quantity. Certain assumptions had to be made concerning

the amount and distribution of solar absorption and infrared cooling in the hurricane. The validity of the results hinges on the correctness of these assumptions. Obviously, more work is needed in this area.

d. Average kinetic energy budget

The magnitude of the terms in the kinetic energy budget equation are presented in Tables 1 and 2 for synoptic Cases I and II, respectively. The entries in these tables represent average values within a 1000-km radius of the cyclone center between 1000 and 100 mb.

In Table 1, the items of interest to note are:

1) The large values for $C(\pi, K_h)$, $H(K_h)$, and $VF(K_h)$ during the first three time periods. The significance of these items has been discussed previously.

2) The total conversion rate of 25.3 watts m^{-2} at 1200 GMT on 2 November compares favorably with estimates obtained by other investigators through the use of the $\omega\alpha$-technique. Some difference should be expected because of the different expression used for conversion in this study. Also, the figures in Table 1 are based on integration to 100 mb, whereas in previous studies the integration was terminated at 300 mb or below.

3) In general, the boundary flux terms are of the same order of magnitude as the conversion term, but slightly smaller. Exceptions to this can be found in layer 3 but, as already pointed out,

errors are more prominent in this layer and the absolute value of the numbers is less reliable.

Table 1. Kinetic energy budget for synoptic Case I. Values in table represent averages in units of watts m^{-2} within a 1000-km radius of the cyclone center. An explanation of the symbols used in the table can be found on p. 23.

DATE	LAYER	$C(\pi, K_h)$	$H(K_h)$	$VF(K_h)$	$D(K_h)$
	1	5.7	1.4	-0.8	-3.3
1200 GMT	2	6.6	3.8	-3.3	
1 Nov.	3	6.4	-19.0	7.6	
	Total	18.7	-13.8	3.5	
	1	4.3	0.6	-0.9	-3.7
0000 GMT	2	5.5	-1.2	3.8	
2 Nov.	3	14.0	-9.0	7.8	
	Total	23.8	-9.6	10.7	
	1	7.8	1.2	-2.1	-6.8
1200 GMT	2	5.5	-1.5	2.3	
2 Nov.	3	12.0	-23.0	10.7	
	Total	25.3	-23.3	7.3	
	1	6.5	1.0	-1.2	-8.7
0000 GMT	2	2.3	-2.5	-0.3	
3 Nov.	3	9.0	-11.0	1.5	
	Total	17.8	-12.5	0.0	
	1	-1.9	1.0	-1.4	-6.4
1200 GMT	2	2.5	1.7	-12.0	
3 Nov.	3	-2.6	1.5	2.9	
	Total	-2.0	4.2	-11.5	
	1	-1.2	-2.1	-0.0	-6.2
0000 GMT	2	6.3	-2.2	0.3	
4 Nov.	3	-7.4	1.0	-5.1	
	Total	-2.3	-3.3	-4.8	

In Table 2, the following items should be noted:

1) The conversion rates in the upper levels of the cyclone are much smaller than in Case I.

Table 2. Kinetic energy budget for synoptic Case II. Values in table represent averages in units of watts m^{-2} within a 1000-km radius of the cyclone center. An explanation of the symbols used in the table can be found on p. 23.

DATE	LAYER	$C(\Pi, K_h)$	$H(K_h)$	$VF(K_h)$	$D(K_h)$
	1	3.8	0.8	-0.4	-2.0
1200 GMT	2	-0.3	3.7	-3.9	
5 Dec.	3	-0.5	11.0	2.4	
	Total	3.0	15.5	-1.9	
	1	4.9	2.0	-1.6	-3.5
0000 GMT	2	-4.2	4.2	-0.8	
6 Dec.	3	4.0	-37.0	14.0	
	Total	4.7	-30.8	11.6	
	1	6.4	3.7	-3.2	-6.5
1200 GMT	2	-4.8	4.8	-12.0	
6 Dec.	3	-0.8	-26.0	13.0	
	Total	0.8	-17.5	-2.2	
	1	7.7	4.1	-0.2	-5.9
0000 GMT	2	-0.4	6.8	-2.8	
7 Dec.	3	8.4	-20.0	4.8	
	Total	15.7	-9.1	1.8	
	1	8.1	7.5	-1.2	-5.7
1200 GMT	2	-0.8	1.7	0.7	
7 Dec.	3	4.2	-2.3	-1.0	
	Total	13.1	6.7	-1.5	
	1	2.7	-0.7	0.3	-3.9
0000 GMT	2	0.4	-0.3	-1.1	
8 Dec.	3	5.8	5.1	-2.6	
	Total	8.9	4.1	-3.4	
	1	3.3	0.2	-0.4	-3.8
1200 GMT	2	0.5	-0.8	-0.1	
8 Dec.	3	4.5	3.4	-0.9	
	Total	9.3	2.8	-1.4	

2) The values of $H(K_h)$ for layer 3 probably are in error at 0000 and 1200 GMT on 6 December, and 0000 GMT on 7 December. The kinetic energy traces shown in Fig. 28b (p. 72) for these dates do not indicate outward transport of kinetic energy of the magnitude indicated by the values in Table 2.

3) The total conversion rate of 15.7 watts m^{-2} at 0000 GMT, 7 December 1969 again compares favorably with estimates of other investigators. It is, however, much smaller than that for Case I; this attests to the fact that the development was much more spectacular in Case I than in Case II.

It should be pointed out that average values present a somewhat distorted picture. For example, in Case I the low-level conversion rates for the first four time periods are 5.7, 4.3, 7.8, and 6.5 watts m^{-2}. In Case II the conversion rates are 3.8, 4.9, 6.4, and 7.7 watts m^{-2}. From these numbers it would appear that the two cases were very similar. However, as was shown previously, the magnitude of the low-level conversion rates were larger in Case II than in Case I even though the average values for the two cases are similar. This averaging process, which has been used in all previous studies, masks the variability of the conversion rates that exists in various parts of the cyclone.

An interesting comparison can be made between this investigation and the one by Eddy (1965). The results for Case I support his findings that the maximum conversion occurs early in the development cycle. However, the results of Case I indicate that the maximum conversion rates were in the upper troposphere rather than in the middle troposphere as Eddy found. Figure 32 shows the vertical profile of conversion rates for each case at the time the most intense cyclogenesis was occurring.

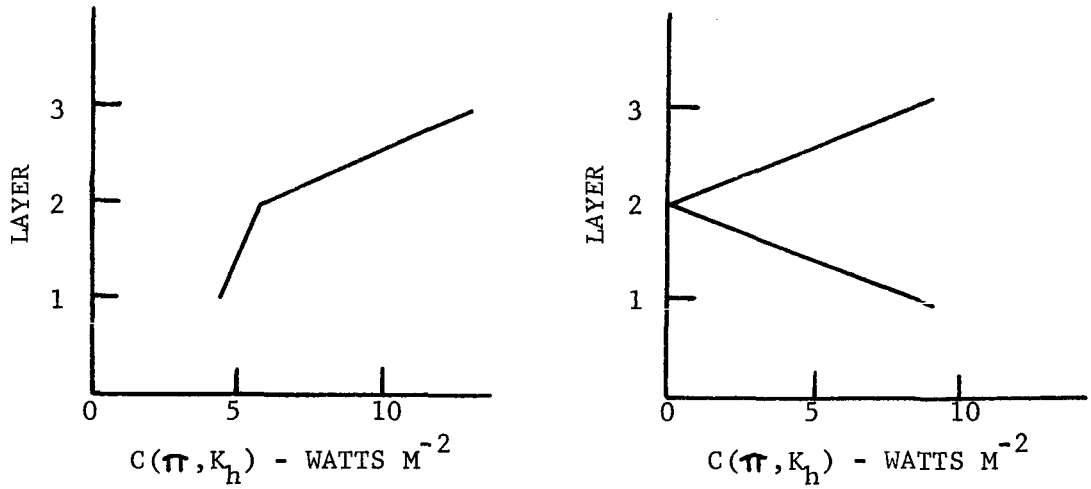

a. 0000 GMT, 2 November 1966 b. 0000 GMT, 7 December 1969

Fig. 32. Vertical profiles of conversion of potential energy into kinetic energy.

The profile for 0000 GMT on 2 November 1966 is very similar to one found by Sechrist and Dutton (1970). On the other hand, the profile for 0000 GMT on 7 December 1969 is more typical of findings by Kung (1966), particularly with respect to the sharp minimum in the profile in the middle layer. From Tables 1 and 2 (pp. 87 and 88) it is apparent also that the vertical profiles vary considerably with time. These examples illustrate the danger of attempting to generalize results based on any single case. While extratropical cyclones are similar in many respects, it is apparent also that each one has distinctive features.

e. Average potential energy budget

The terms of the potential energy budget equation are presented in Tables 3 and 4 for synoptic Cases I and II, respectively. The terms representing the generation of potential energy by diabatic processes, and the conversion of potential energy into kinetic energy, already have been discussed in some detail. The remaining terms of the potential energy budget now will be considered.

1) Boundary flux of potential energy. - It is apparent immediately in Tables 3 and 4 that the boundary flux terms are very large. In general, the two components, $H(\pi)$ and $VF(\pi)$, are nearly equal in magnitude, but opposite in sign. Therefore, small errors in either component may result in a large error in the total flux term which is the sum of $H(\pi)$ and $VF(\pi)$. The magnitude of the flux terms also demonstrates the futility of attempting to compute changes in kinetic energy from corresponding changes in potential energy. An error of only 10% in computing the potential energy flux terms could result in errors in the potential energy budget of 700 to 800 watts m^{-2}, which is one to two orders of magnitude larger than any of the terms in the kinetic energy budget equation.

It should be noted that the potential energy flux terms generally are much smaller in layer 2 than in either of the other two layers. This tendency can be observed in the values in Tables 3 and 4 for both synoptic cases. This fact seems to indicate th-

the conditions in layer 2 were more nearly barotropic and geostrophic than in the other two layers resulting in a smaller advection of temperature, hence a smaller advection of potential energy.

Table 3. Total potential energy budget for synoptic Case I. Values in table represent averages in units of watts m^{-2} within a 1000-km radius of the cyclone center. An explanation of the symbols used in the table can be found on p. 23.

DATE	LAYER	$G(\pi)$	$-C(\pi, K_h)$	$H(\pi)$	$VF(\pi)$	$C(\pi, \pi')$
	1	-120	-5.7	2500	-2600	-29
1200 GMT	2	82	-6.6	490	-380	31
1 Nov.	3	-350	-6.4	-4100	3900	-57
	Total	388	-18.7	-1110	920	55
	1	77	-4.3	3300	-2500	230
0000 GMT	2	-43	-5.5	-580	760	50
2 Nov.	3	-230	-14.0	-2000	1800	-57
	Total	-196	-23.8	720	60	223
	1	9	-7.8	4900	-3600	370
1200 GMT	2	80	-5.5	-1200	1700	140
2 Nov.	3	-430	-12.0	-2700	2500	-57
	Total	-341	-25.3	1000	600	453
	1	60	-6.5	1100	-1100	0
0000 GMT	2	80	-2.3	-260	400	39
3 Nov.	3	-57	-19.0	310	-230	23
	Total	83	-27.8	1150	-930	62
	1	140	1.9	2000	-2300	-86
1200 GMT	2	79	-2.5	1000	-1500	-143
3 Nov.	3	710	2.6	2100	-2000	29
	Total	929	2.0	5100	-5800	-200
	1	38	1.9	1300	-900	114
0000 GMT	2	-85	-2.5	-2600	2000	-172
4 Nov.	3	-120	2.6	1000	-1800	-229
	Total	-267	2.0	-300	-700	-287

Table 4. Total potential energy budget for synoptic Case II. Values in table represent averages in units of watts m^{-2} within a 1000-km radius of the cyclone center. An explanation of the symbols used in the table can be found on p. 23.

DATE	LAYER	$G(\pi)$	$-C(\pi, K_h)$	$H(\pi)$	$VF(\pi)$	$C(\pi,\pi')$
	1	-35	-3.8	4000	-3100	258
1200 GMT	2	67	0.3	1600	-1600	0
5 Dec.	3	300	0.5	1700	-450	358
	Total	332	3.0	7300	-4150	616
	1	210	-4.9	8600	-7900	200
0000 GMT	2	300	4.2	750	1100	530
6 Dec.	3	460	-4.0	-4900	5600	200
	Total	970	-4.7	4450	-1200	930
	1	160	-6.4	7600	-7200	114
1200 GMT	2	330	4.8	420	810	352
6 Dec.	3	250	0.8	-3200	4500	372
	Total	740	-0.8	4820	-1890	838
	1	140	-7.7	3000	-2500	144
0000 GMT	2	180	0.4	-370	690	228
7 Dec.	3	-360	-8.4	-2100	2900	86
	Total	-40	-15.7	530	1090	458
	1	250	-8.1	1400	-1100	86
1200 GMT	2	220	0.8	220	-720	-143
7 Dec.	3	-1100	-4.2	-930	950	5
	Total	-630	-13.1	690	-870	-52
	1	130	-2.7	240	290	152
0000 GMT	2	140	-0.4	840	-1300	-132
8 Dec.	3	1100	-5.8	2400	-1700	200
	Total	1370	-8.9	3480	-2710	220
	1	-21	-3.3	1800	-1400	104
1200 GMT	2	36	-0.5	-230	-47	-79
8 Dec.	3	710	-4.5	1700	-1800	-29
	Total	725	-9.3	3270	-3247	6

2) Interaction of the cyclone with larger scales of motion. - The term $C(\pi, \pi')$ which appears in the potential energy budget equation provides a unique means to study the interaction of a cyclone with the larger scales of motion. The average values of $C(\pi, \pi')$ for each synoptic case are shown in Tables 3 and 4 (pp. 92 and 93).

In synoptic Case I, the values of $C(\pi, \pi')$ for the entire layer, 1000 to 100 mb, are large and positive during the early periods of cyclogenesis, thus indicating that the potential energy of the cyclone is being increased at the expense of potential energy in the atmospheric volume surrounding the cyclone. After 1200 GMT on 2 November 1966, the values of $C(\pi, \pi')$ decrease and eventually become negative, which indicates a reverse flow of potential energy.

By contrast, the values of $C(\pi, \pi')$ for the total layer in Case II are positive throughout almost the entire life of the cyclone. The only exception is at 1200 GMT on 7 December 1969 at which time a value of -52 watts m^{-2} can be noted. As with Case I, the values do decrease with time but never reach the large negative values attained in Case I. The values of $C(\pi, \pi')$ are much larger in Case II than in Case I during the early development stage; this suggests that the interaction of the cyclone with the larger scales of motion played a more important role in cyclogenesis in Case II than in Case I.

To the author's knowledge, this is the first time that the term $C(\pi, \pi')$ has been evaluated in an energy budget study of this type. Therefore, the extent to which the results just described apply to other cyclones cannot be determined by comparison with other studies.

6. CONCLUSIONS

A method has been presented to investigate the atmospheric energy budget as related to cyclogenesis. This work represents an extension of previous studies in that all of the terms of the energy budget equation were evaluated throughout the development period of the cyclone. Also, objectively analyzed data were used in the evaluation of the energy budget terms in order to minimize systematic errors. An objective analysis scheme is described that insures that all of the resolution contained in the rawinsonde observations is incorporated in the analyses.

The energy budget equations used in the present research were patterned after those suggested by Smith (1970), but were modified to include the hydrostatic approximation and the use of pressure as the vertical coordinate rather than height. These equations have been shown to be advantageous because the individual terms represent basic physical processes which produce changes in atmospheric energy, and the equations provide a means to study the interaction of the cyclone with the larger scales of motion.

Two examples of cyclogenesis over the eastern United States were chosen for study. One of the cases (1-4 November 1966) represented an example of vigorous development, while the development in the other case (5-8 December 1969) was more modest. While computational errors may be serious due to errors in the measured data, particularly in the higher levels of the atmosphere, it is

felt that the results of this study present a representative picture of energy processes during cyclogenesis. The major conclusions that are evident from the present research are as follows:

1) Diabatic processes can be sufficient to offset a major portion of the frictional dissipation of the cyclone and in some cases may contribute to the initial development of the cyclone. Diabatic processes were significant in both of the synoptic cases that were considered in this paper.

2) The downward transport of kinetic energy from the jet stream level can be an important source of energy for a developing cyclone. This factor was significant in one of the synoptic cases, but not in the other, which implies that downward transport of kinetic energy is not a necessary condition for cyclogenesis.

3) In general, the conversion rates determined in this study compared favorably with those found in previous studies. However, it was shown that the $\omega\alpha$-technique of computing conversion rates that was used in most of the previous studies may produce erroneous results because of the omission of boundary terms. In fact, the results of the present research clearly indicate that the validity of any energy budget study of a limited region of the atmosphere hinges upon the extent to which boundary fluxes of energy can be determined. In general, the boundary flux terms are the same order of magnitude as the conversion terms and cannot be neglected.

In addition to the above conclusions, other items of interest to note from the present research are as follows:

1) The interaction of the cyclone with the surrounding atmosphere was found to be an important factor in the potential energy budget for both of the synoptic cases considered.

2) When the terms of the energy budget equations are averaged in time and space, some of the spurious fluctuations in the data are eliminated, but at the same time some of the real variability that exists in various parts of the cyclone is masked.

3) It is difficult, if not impossible, to draw generalized conclusions from the study of one or two cyclones because of the marked variability than can exist between energy processes in different cyclones.

7. RECOMMENDATIONS FOR FURTHER RESEARCH

It is likely that further studies of the type presented here can contribute substantially to the understanding of atmospheric energetics as related to cyclogenesis. The approach presented in this study should be extended to include partitioning of the diabatic heating term into individual components resulting from latent heat release, sensible heat transfer, radiational losses, etc. The results concerning the interaction of cyclones with the larger scales of motion must be considered tentative at this point. Further research could determine the extent to which other cyclones interact with global motions.

The main limiting factor in energy budget studies continues to be the lack of adequate observations, both in number and accuracy. Very precise measurements are required in order to determine accurately vertical motions and boundary fluxes of energy. The Global Atmospheric Research Program may provide a source for observations that are more suitable for energy budget studies than currently exist. These data should become available in the mid 1970's.

REFERENCES

Anthes, R. A., and D. R. Johnson, 1968: Generation of available potential energy in Hurricane Hilda (1964). Mon. Wea. Rev., 96, 291-302.

Barnes, S. L., 1964: A technique for maximizing detail in numerical weather map analysis. J. Appl. Meteorol., 3, 396-409.

Barr, S., W. K. Widger, Jr., I. A. Miller and R. Stanton, 1971: Objective subsynoptic upper level analysis. J. Appl. Meteorol., 10, 410-417.

Bullock, B. R., and D. R. Johnson, 1971: The generation of available potential energy by latent heat release in a mid-latitude cyclone. Mon. Wea. Rev., 99, 1-14.

Charney, J. G., 1947: The dynamics of long waves in a baroclinic westerly current. J. Meteorol., 4, 135-162.

Cressman, G. P., 1959: An operational objective analysis system. Mon. Wea. Rev., 87, 367-374.

Danard, M. B., 1964: On the influence of released latent heat on cyclone development. J. Appl. Meteorol., 3, 27-37.

Danard, M. B., 1966: On the contribution of released latent heat to changes in available potential energy. J. Appl. Meteorol., 5, 81-84.

Dutton, J. A., and D. R. Johnson, 1967: The theory of available potential energy and a variational approach to atmospheric energetics. Advances in Geophysics, Vol. 12, New York, Academic Press, 333-436.

Eddy, A., 1965: Kinetic energy production in a mid-latitude storm. J. Appl. Meteorol., 4, 569-575.

Hess, S. L., 1959: Introduction to Theoretical Meteorology. New York, Holt, Rinehart and Winston Book Co., 362 pp.

Holopainen, E. O., 1963: On the dissipation of kinetic energy in the atmosphere. Tellus, 15, 26-32.

Johnson, D. R., 1970: The available potential energy of storms. J. Atmos. Sci., 27, 727-741.

Kung, E. C., 1966: Kinetic energy generation and dissipation in the large-scale atmospheric circulation. Mon. Wea. Rev., 94, 67-82.

Kuo, H. L., 1949: Dynamic instability of two-dimensional non-divergent flow in a barotropic atmosphere. J. Meteorol., 6, 105-122.

Lettau, H., 1954: Notes on the transformation of mechanical energy from and to eddying motion. J. Meteorol., 11, 196-201.

Lettau, H., 1959: Wind profile, surface stress and geostrophic drag coefficients in the atmosphere surface layer. Advances in Geophysics, 6, 241-255.

Lorentz, E. N., 1955: Available potential energy and the maintenance of the general circulation. Tellus, 7, 157-167.

Miller, J. E., 1950: Energy transformation functions. J. Meteorol., 7, 152-159.

Miller, J. E., 1951: Energy equations. Compendium of Meteorology, Boston, Amer. Meteorol. Soc., 483-491.

Oort, A. H., 1964: On estimates of the atmospheric energy cycle. Mon. Wea. Rev., 92, 483-493.

O'Brien, J. J., 1970: Alternate solution to the classical vertical velocity problem. J. Appl. Meteorol., 9, 197-203.

O'Neill, T. H. R., 1966: Vertical motion and precipitation computations. J. Appl. Meteorol., 5, 595-605.

Palmén, E., 1958: Vertical circulation and release of kinetic energy during the development of hurricane Hazel into an extratropical storm. Tellus, 10, 1-23.

Palmén, E., and O. Holopainen, 1962: Divergence, vertical velocity and conversion between potential and kinetic energy in an extratropical disturbance. Geophysica, 8, 89-112.

Palmén, E., and C. W. Newton, 1969: Atmospheric Circulation Systems. New York, Academic Press, 603 pp.

Petterssen, S., 1956: Weather Analysis and Forecasting. Vol. I. Motion and Motion Systems. New York, McGraw-Hill Book Co., 428 pp.

Pfeffer, R. L., 1957: On the physical significance of energy transformation functions. Studies of Atmospheric General Circulation II, Dept. of Meteorology, M.I.T., Final Rept., General Circulation Project.

Richardson, L. F., 1922: Weather Prediction by Numerical Process. Cambridge University Press, 236 pp. Reprint, with a new introduction by Sidney Chapman: New York, Dover Publications, 1965, 236 pp.

Sechrist, F. S., and J. A. Dutton, 1970: Energy conversions in a developing cyclone. Mon. Wea. Rev., 98, 354-362.

Shuman, F. G., 1957: Numerical methods in weather prediction: II. Smoothing and filtering. Mon. Wea. Rev., 85, 357-361.

Smith, P. J., 1969: On the contribution of a limited region to the global energy budget. Tellus, 11, 202-207.

Smith, P. J., 1970: A note on energy conversions in open atmospheric systems. J. Atmos. Sci.,27, 518-521.

Smith, P. J., and L. H. Horn, 1969: A computational study of the energetics of a limited region of the atmosphere. Tellus, 11, 193-200.

Spar, J., 1950: Synoptic studies of the potential energy in cyclones. J. Meteorol., 7, 48-53.

Thompson, P. D., 1961: Numerical Weather Analysis and Prediction. New York, Macmillan Co., 170 pp.

Van Mieghem, J., 1951: Applications of thermodynamics of open systems to meteorology. Compendium of Meteorology, Boston, Amer. Meteorol. Soc., 531-538.

White, R. M., and B. Saltzman, 1956: On the conversion between potential and kinetic energy in the atmosphere. Tellus, 8, 357-363.

Wiin-Nielsen, A., 1964: On energy conversion calculations. Mon. Wea. Rev., 92, 161-167.

Wiin-Nielsen, A., 1968: On the intensity of the general circulation of the atmosphere. Rev. Geophys., 6, 559-579.